國立交 通 大 學

材料科學與工程學系

碩 士 論 文

以濺鍍技術製備 ITO 透明導電薄膜成長在不同基材其應力行爲及基材效應對其光學性質之研究

The Investigation of Stress Behavior of Sputtered Indium Tin Oxide (ITO) Thin Films on Various Substrates and Substrate Effect on Optical Properties of ITO Film

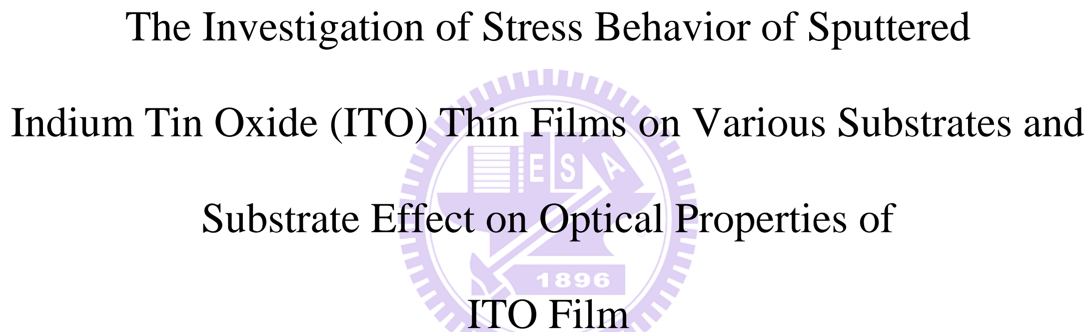

研 究 生：Vu Hong Hanh

指導教授：呂志鵬　博士

中 華 民 國 一百 年 七 月

以濺鍍技術製備 ITO 透明導電薄膜成長在不同基材其應力行爲及基材效應對其光學性質之研究

The Investigation of Stress Behavior of Sputtered Indium Tin Oxide (ITO) Thin Films on Various Substrates and Substrate Effect on Optical Properties of ITO Film

研 究 生：武紅幸　　Student：Vu Hong Hanh

指導教授：呂志鵬　　Advisor：Dr. Jihperng (Jim) Leu

國 立 交 通 大 學

材 料 科 學 與 工 程 學 系

碩 士 論 文

A Thesis

Submitted to Department of Materials Science and Engineering College of Engineering

National Chiao Tung University

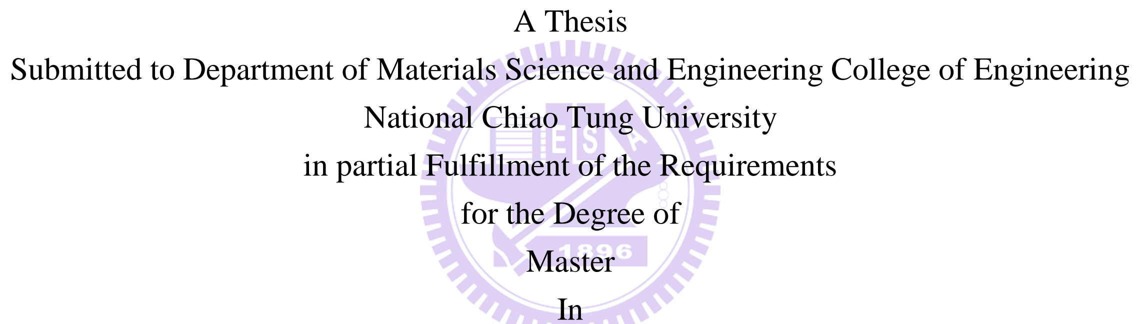

in partial Fulfillment of the Requirements

for the Degree of

Master

In

Materials Science and Engineering

July 2011

Hsinchu, Taiwan, Republic of China

中華民國一百年七月

以濺鍍技術製備 ITO 透明導電薄膜成長在不同基材其應力行爲及基材效應對其光學性質之研究

學生: 武紅幸　　　　　　　　　　　　　　　　　指導教授:呂志鵬 博士

國 立 交 通 大 學
材料科學與工程學系碩士班
碩 士 論 文

摘　要

ITO(Indium Tin Oxide) 是具有高導電性且於可見光範圍內具備高透明特性之材料，普遍廣泛被應用於光電產業及研究方面上。近年來隨可撓性光電元件之發展，爲求輕量化及薄型化，以高分子材料作爲元件之基板則有受到愈來愈多討論與重視之趨勢，這是由於它們具有質輕、價廉、耐衝擊、可製備成各種尺寸且具有可撓性等優勢。然而，在於塑膠基板上鍍覆透明導電膜(ITO),所造成之問題在於導電膜內造成明顯應力之形成，主要問題源自於高分子基材之高熱膨脹係數；由於塑膠基板與ITO之間的熱膨脹係數差異將會造成薄膜產生應力方面的問題，過量應力之存在往往造成ITO薄膜導電度不佳、透明度下降、表面破裂或其它缺陷，進而使得元件可靠度不佳甚而整個失效。因此，對於ITO膜沉積於不同基材上其應力行爲之了解對其元件應用及其可靠度之關係逐漸形成高度重視之議題。

本論文主要探討以直流式濺鍍系統法(DC Sputter Stystem),於不同基材包含矽(Si)、聚对苯二甲酸乙二酯 (PET) 及聚醯亞胺 (PI) 薄膜上沉積ITO膜，利用真空彎柄儀(Bending Beam System)在於溫度循環測試下探討其應力行爲。實驗結果顯示，室溫下所沈積ITO膜在於不同基材形成之殘留應力皆呈現張應力，然而應力值大小決定於基材之楊氏係數，兩者之間有強烈之關係。沉積於PET高分子基材時ITO膜具有最小應力之形成，然而在於Si基材上具有最大之應力值其範圍爲80~330MPa。不同之應力形成主要在於高分子基材具備較低楊氏係數因而在於沉積過程中基材產生塑性變形進而減低ITO膜內應力之產生。進一步結果顯示ITO膜在於高分子基材上所造成表面破裂之臨界應力值分別於PET上爲19.2MPa及在於PI上爲75MPa。

本研究同時進一步討論製程溫度之影響。提高沉積溫度至200℃，分別在於Si及PI兩種不同基材。有別於室溫下所沉積之ITO膜，結果顯示提高製程溫度將明顯降低其應

力值，主要因素可歸咎於在於高溫製程下將提高離子轟擊效應及增加導電膜內結晶程度之改善。

其次本論文研究ITO膜在於不同基材上在於可見光範圍內其穿透度及帶狀能隙距離的大小(band gap)，探討基材效應所造成之應力對其光學性質之影響。利用UV-VIS光譜儀量測結果顯示ITO膜在於三種不同基材(glass, PET及PI)在於可見光範圍內其穿透度皆為接近90%。而在於band gap量測上發現當ITO在於高分子基材上時其能隙距離有窄化之趨勢。於兩種不同之高分子基材比較上，ITO/PET具有較大之能隙主要具有較低之張應力，意謂當應力值被提升時，帶狀能隙距離的大小亦隨之降低。

The Investigation of Stress Behavior of Thin Sputtered Indium Tin Oxide (ITO) Films on Various Substrates and Substrate Effects on Optical Properties of ITO Film

Student: Vu Hong Hanh Advisor: Dr. Jihperng (Jim) Leu

Department of Materials Science and Engineering

National Chiao Tung University

Abstract

Indium tin oxide (ITO) is a common transparent conductive layer in optoelectronic devices because of its high electrical conductivity and transparent in visible wavelength. Recently, with the development of flexible optoelectronic devices, polymer material is widely employed as the substrate in these devices due to its potential advantages of high flexibility, low cost, and light weight. However, once ITO film is formed onto polymer substrate, there is a significant stress induced in the ITO film because of polymer's high coefficient thermal of expansion (CTE). A large film stress may result in poor durability, low conductivity, or low transparency. Thus, understanding the ITO film stress behavior onto various substrates is highly needed for its applications and reliability in flexible devices.

In this study, the DC sputtered ITO film stress as a function of deposition temperature was investigated under multiple thermal cycling by using a bending beam technique. On various substrates such as Si, polyethylene terephthalate (PET) and ODPA-BAPP polyimide

(PI), the room temperature formed ITO films exhibit a tensile stress. It was found that the film stress level strongly depends on the Young's modulus of substrate. ITO stress achieves the lowest level as the film was deposited on PET. ITO film on Si has highest stress in the range of 80 – 330 MPa. The difference in stress level of ITO on various substrates is due to the fact that polymer substrate with lower Young's modulus can plastically deform under ITO film stress, resulting in stress reduction of the ITO film. The critical stresses for cracking of ITO on polymer substrates were obtained as well, 19.2 MPa for ITO/PET and 75 MPa for ITO/PI, respectively.

Different from the ITO films deposited at room temperature, ITO films deposited at 200 ℃ on Si and PI are under less tensile stresses. The compressive tendency of film stress with increase in the deposition temperature can be attributed to a stronger ion peening effect and an improvement of film crystallinity.

Beside the study of film stress behavior, transmittance and optical band gap of ITO film on glass, PET and PI substrates were investigated in order to understand any substrate effect on these importance characteristics of ITO film. An UV-visible spectrophotometer system was used to examine the transmittance of ITO film. The results show that ITO films on glass, PET and PI have similar transmittance nearly 90 % in the visible light region. However, the film optical band gap tends to narrow when coating on polymer substrates. Moreover, ITO on PET has larger optical band gap than ITO on PI presumably due to the less tensile stress of

film on PET substrate.

Acknowledgements

Firstly, I owe my deepest gratitude to my advisor, Dr. Jihperng Leu, who gave me such great opportunity to study abroad. I am heartily thankful to him for his guidance, understanding, patience and attention to me during the time I study in Taiwan. Without his support, this thesis would not have been possible.

Secondly, I am indebted to my seniors, Tai Yin Lin, Sky Hsu, and Le Huu Phuoc, who gave me a lot of useful suggestion in both study and real life. I also owe my honest thankfulness to Anthony for his help in the deposition of ITO films, and to Kima, who helped me so much in XRD study of ITO film.

Thirdly, I would like to show my sincere thankfulness to all seniors, friends and juniors in NIP lab, who are very friendly and kindly to me. They helped me easily adapt to the life in Taiwan. I also wish to thank to all Vietnamese students in NCTU, who shared and enjoyed the life in Taiwan with me.

Lastly, but not least importantly, I am grateful to thank my parents, my brother and sister for their great love and encouragement. To them, I dedicate this thesis.

Contents

摘　要 I

Abstract III

Acknowledgements VI

Contents VII

List of Tables IX

List of Figures X

Chapter 1 Introduction 1

1.1 Background 1

1.2 Thesis outline 5

Chapter 2 Literature review 6

2.1 General theory of film stress 6

2.2.1 Intrinsic stress 8

2.1.2 Thermal stress 11

2.2 Optical properties of ITO films 12

2.3 Effects of the stress on film properties 14

Chapter 3 Experimental 16

3.1 Sample preparation 16

3.1.1 Substrate preparation 16

3.1.2 Indium tin oxide layer deposition 21

3.2 Experimental procedures 22

3.3 Instrumentation 24

3.3.1 Bending beam system 24

3.3.2 Scanning electron microscope 30

3.3.3 X-ray diffraction 32

3.3.4 Hall Effect measurement 33

3.3.5 UV-visible spectrophotometer system 34

Chapter 4 Results and discussion 35
4.1 Thermo-mechanical parameters of ITO film and substrates 35
4.2 Stress behavior of ITO film deposited on Si substrate 37
4.2.1 Stress of ITO film deposited at room temperature on Si substrate.......................... 37
4.2.2 Stress of ITO film deposited at 200 ℃ on Si substrate 42
4.3 Stress of ITO film on ODPA-BAPP polyimide substrate 48
4.3.1 Stress behavior of ODPA-BAPP polyimide film on silicon substrate 48
4.3.2 Stress of ITO film deposited at room temperature on polyimide substrate............. 51
4.3.4 Stress of ITO film deposited at 200 ℃ on PI substrate 56
4.4 Stress of ITO film on PET substrate.. 62
4.4.1 Stress of PET film on silicon substrate.. 62
4.4.2 Stress of ITO film deposited at room temperature on PET substrate...................... 66
4.5 Effect of substrates on the stress of ITO film... 70
4.6 Critical stress for damage of ITO film on polymer substrates 72
4.7 Effects of substrate on the optical properties of ITO films 75
Chapter 5 Conclusion 79
References 82

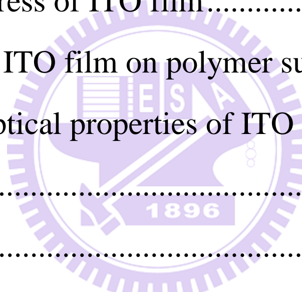

List of Tables

Table 3. 1 Condition of ITO film deposition 21
Table 3. 2 The list of samples 21
Table 4. 1 Thermo-mechanical properties of ITO film and various substrates 36
Table 4. 2 The stress comparison for the ITO films deposited at room temperature and 200℃ 46
Table 4. 3 Summary effect of substrate temperature on ITO/PI stress behavior 59
Table 4. 4 Summary stress of ITO films on various substrates 71
Table 4. 5 Optical band gap of ITO in the relationship with film stress and carrier concentration 78

List of Figures

Figure 1. 1 Morphology of cracked film 4
Figure 1. 2 Morphology of buckled film 4
Figure 2. 1The films are under tensile and/ or compressive stress [28] 7
Figure 3. 1 Chemical structure of PET 19
Figure 3. 2 Chemical structure of TFA solvent 19
Figure 3. 3 Chemical structure of ODPA 19
Figure 3. 4 Chemical structure of BAPP 19
Figure 3. 5 Chemical structrure of DMAc 20
Figure 3. 6 Temperature – time profile for curing of polyimide 20
Figure 3. 7 Chemical structure of ODPA-BAPP polyimide 20
Figure 3. 8 Flow chart of experiment procedures 23
Figure 3. 9 Diagram of bending beam system 26
Figure 3. 10 Principle to determine the bending curvature of sample[60] 27
Figure 3. 11 Spatial relationship among parameters in Eq. (3.8) 29
Figure 3. 12 Schematic diagram of an SEM 31
Figure 3. 13 Definition of the angle of incidence and diffraction in an XRD experiment 32
Figure 4. 1 Stress of room – temperature deposited ITO film on Si substrate 40
Figure 4. 2 The SEM top-view images of ITO films (a) as-deposited, (b) after the 1st thermal cycle, and (c) after the 2nd thermal cycle 41
Figure 4. 3 The morphology of (a) as-deposited ITO film and (b) post-deposited ITO film 41
Figure 4. 4 Stress-temperature curve of 200℃-deposited ITO film on Si substrate 45
Figure 4. 5 XRD patterns of ITO film deposited on Si substrate at room temperature and 200 ℃ 46
Figure 4. 6 Surface morphology of ITO/Si sample (a) as-deposited and (b) after thermal cycling 47
Figure 4. 7 Stress behavior of ODPA-BAPP polyimide film on silicon substrate 50
Figure 4. 8 Stress vs. temperature of ITO film deposited at room temperature onto ODPA-BAPP polyimide 53
Figure 4. 9 XRD pattern of ITO film on PI substrate before and after stress measurement 54
Figure 4. 10 Surface morphology of ITO/PI sample (a) before thermal cycling, and (b) after thermal cycling 55
Figure 4. 11 Stress vs. temperature of ITO film deposited on ODPA-BAPP polyimide substrate at 200℃ 59

Figure 4. 12 XRD pattern of ITO deposited at room temperature and 200 ℃ on PI substrate 60
Figure 4. 13 SEM top-view of ITO film on ODPA-BAPP polyimide substrate: (a) Room temperature deposited film; (b) 200 ℃-deposited film 60
Figure 4. 14 Surface morphology of ITO/PI sample (a) as-deposited and (b) after the thermal cycling 61
Figure 4. 15 Stress vs. temperature of PET film on Si substrate 65
Figure 4. 16 Stress-temperature curve of ITO film deposited at room temperature onto PET substrate. 69
Figure 4. 17 Surface morphology of ITO/PET sample (a) as-deposited and (b) after thermal cycling 69
Figure 4. 18 Stress vs. temperature of ITO on PET within 30 – 100 ℃ 73
Figure 4. 19 Surface morphology of ITO/PET (a) before stress measurement and (b) after stress measurement within 30 – 100 ℃ 73
Figure 4. 20 Stress vs. temperature of ITO/PI within 30 – 250 ℃ 74
Figure 4. 21 Surface morphology of ITO/PI (a) before stress measurement and (b) after stress measurement within 30 – 250 ℃ 74
Figure 4. 22 Transmittance of ITO films on glass, PET and PI in the visible light 77
Figure 4. 23 Optical band gap of ITO film on glass, PET and PI substrates 78

Chapter 1 Introduction

1.1 Background

Indium tin oxide (ITO), an n-type semiconductor material, is widely used as a transparent conductive layer in photovoltaic devices[1-3], and an electrode for displays[4-7] owing to its superior optical and electrical properties of high transmittance in the visible light region and low resistivity. In these devices, ITO film is commonly deposited on glass substrate [8-10] because of its high transparency and low cost. However, glass is brittle, heavy and rigid, making it not suitable for certain applications, where flexibility, light weight, and toughness are required. To solve this issue, polymers with the advantages of low cost, light weight, and excellent bendability have been recently used as a replacement for glass [11-14]. Among various candidate materials of polymer substrates, polyethylene terephthalate (PET) and polyethylene naphthalate (PEN) are commonly used for flexible device because they are easily fabricated and cheap. However, their glass transition temperatures (Tg) are relatively low, 74.5 °C for PET and 150 °C for PEN[15, 16]. Hence, on these substrates, ITO can be only deposited and/ or treated at temperature below the T_g of substrates. Low temperature deposited ITO film generally has high resistance and poor transparency, which are two important performance factors for optoelectronic devices applications. Nowadays, polyimide

(PI) with high T_g (≥ 200 °C) [17] is attracting researchers' attentions and becomes a good substitute for PET and PEN.

As ITO films are deposited on substrates, the film stress is generated due to the materials mismatch between the film and the substrate [18]. Generally, film stress is built up by two components; namely intrinsic stress and thermal stress [19, 20]. Intrinsic stress is caused from the mismatch in microstructure between film and substrate during the film deposition. Thermal stress is formed due to the difference in CTE between the film and the substrate [21]. Film stress is categorized into two types: (1) compressive stress causes convex film; (2) tensile stress results in concave film. Once the film stress reaches a threshold stress value, it may cause film cracking (if tensile stress) or buckling (if compressive stress) as shown in Figures 1.1 and 1.2, respectively [22, 23]. In the cracked film, the carrier mobility is sufficiently reduced, leading to a high resistivity film. If buckling is formed, the film becomes less transparent due to more scattered photons. To fabricate devices of high quality, the optimization of stacked film stress is highly desirable. Therefore, it is important to understand the stress behavior of ITO on various substrates under thermal cycling, similar to the thermal process post ITO film deposition in the fabrication of devices. It is also of interests to understand the integrity of stacked films and methodology for retaining the film quality. Thus, the objectives of this thesis can be summarized below:

(1) To study the dependence of ITO film stress on various substrates (Si, PET and PI).

(2) To study the effect of deposition temperature on ITO stress on various substrates (Si, PET, and PI).

(3) To investigate the critical stress values for inducing damages of ITO films on polymer substrates (PET and PI).

(4) To study the effect of substrate on the optical properties of ITO film.

In specific, a bending beam technique is used on this thesis to measure the stress of DC sputtered ITO films for studying the behavior of film stress on various substrate, such as Si, PET and ODPA-BAPP polyimide (PI). Among these substrates, PET and PI films are intended for flexible devices, while Si is only used for the stress measurement because of its high reflectivity as required by the bending beam stress measurement. ITO films on PET were only formed at room temperature due to PET's low glass transition, T_g ~ 75 ℃. In contrast, ITO films were deposited on Si and ODPA-BAPP polyimide (T_g at 230 ℃) at both room temperature and 200 ℃ to study the dependence of ITO and ITO/polymer film stress on deposition temperature. The glass transition of polymers restricts the highest temperature condition in the stress measurement. Therefore, the stress of ITO on Si and ITO/PI on Si are examined with thermal cycles from 30 ℃ to 200 ℃. However, the stress measurement of ITO/PET on Si is only carried out from room temperature to 70 ℃. In this study, the optical properties of ITO are tested by UV-visible spectrophotometer system for examining the effect of substrate on these properties as well.

Figure 1. 1 Morphology of a cracked ITO film on PET

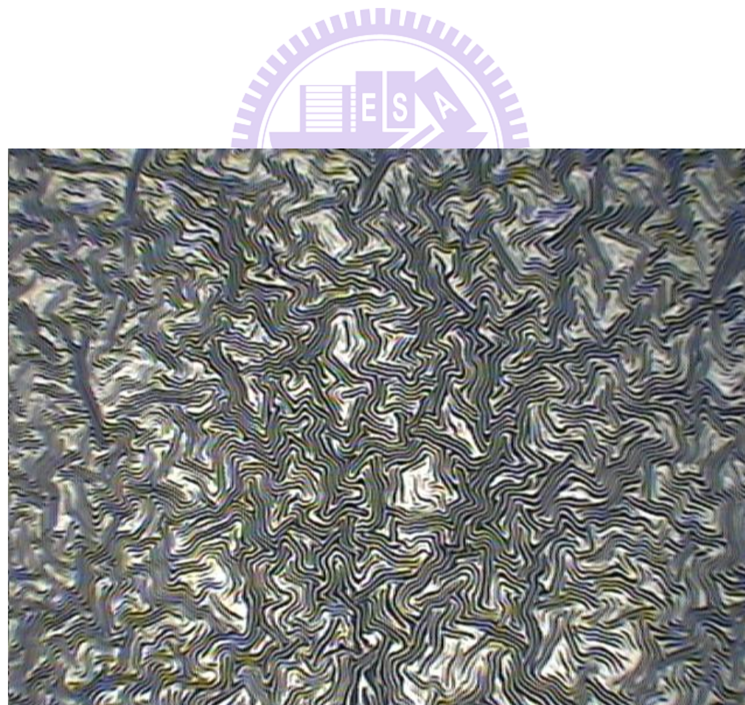

Figure 1. 2 Morphology of a buckled ITO/PET layered structure

1.2 Thesis outline

Toward the understanding of ITO film stress behavior and its effect on film properties, this thesis is organized into five chapters.

(1) Chapter 1 is a brief introduction about this thesis.

(2) Chapter 2 presents the review of the general theory of ITO film, such as film stress, and optical properties.

(3) Chapter 3 details the sample preparation and introduces the instruments which are used for measurements in this thesis.

(4) Chapter 4 describes the stress measurement results and the substrate-dependence of ITO film optical properties.

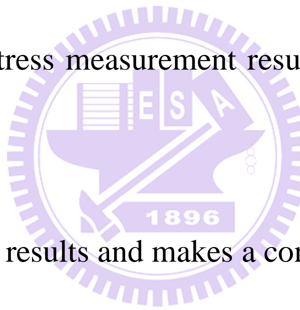

E S A
1896

(5) Chapter 5 summarizes the results and makes a conclusion for the thesis.

Chapter 2 Literature review

2.1 General theory of film stress

Residual stress in coated film is an inevitable occurrence because the differences in mechanical and thermal properties exist between the film and the substrate [24]. Generally, film stress is built up from two components as described in Eq. (2.1) [19, 27]

$$\sigma_r = \sigma_{in} + \sigma_{th} \tag{2.1}$$

where σ_{in} is the intrinsic stress and σ_{th} is the thermal stress. The stress value may be negative or positive. The negative stress value means the film is under a compressive stress or the substrate is convex. Oppositely, the film is under a tensile stress or the substrate is concave if the stress value is positive. An example of a film/substrate system with tensile or compressive film is shown in Figure 2.1

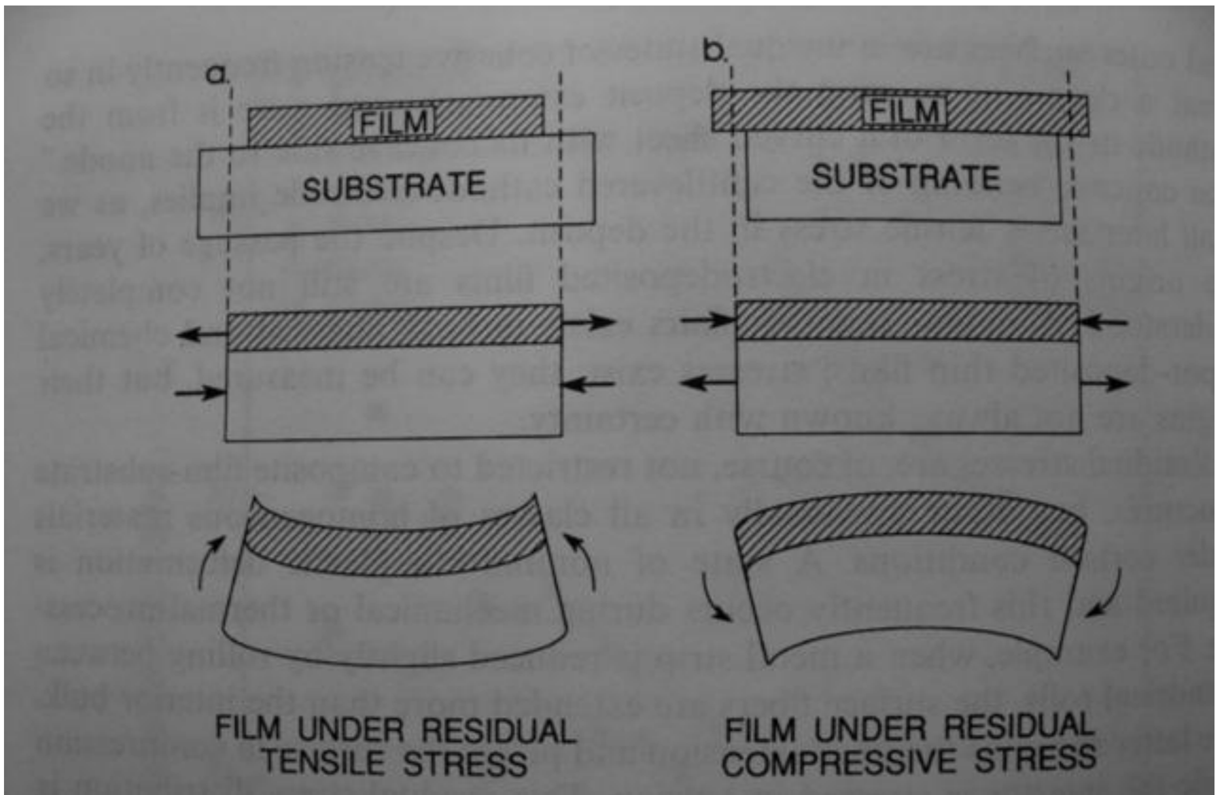

Figure 2. 1 The films are under tensile and/ or compressive stress [28]

2.2.1 Intrinsic stress

Intrinsic film stress is introduced and built up in the film during the deposition due to the mismatch in microstructure between film and substrate. The stress is tensile or compressive depending on the film deposition conditions such as deposition method, substrate temperature, working pressure, gas type, and gas ratio, etc. For example, the stress of a sputtered ITO film is generally compressive stress, however, it tends to tensile stress when increasing working pressure[29, 30]. Chen *et al.*[31] reported that the stress of ITO film formed by vapor chemical deposition also changes from compressive to tensile stress with increasing substrate temperature. The generation mechanism of intrinsic stress might be affected by three main effects: atomic peening effect, recrystallization effect, and island coalescence effect.

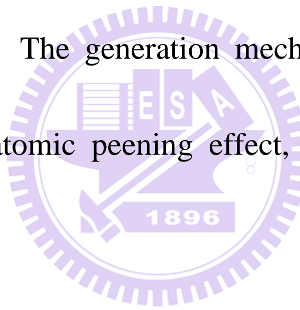

(1) Atomic peening effect

In sputtered film, the compressive intrinsic stress is generally produced by the atomic peening effect. This is attributed to the lattice distortion produced by bombardment of the growth film by the energetic sputtered and reflected gas atoms. Since a higher gas pressure favors more atomic collision, the initially high energy of sputtered and reflected atoms is dissipated and the stress is thus reduced. The stress eventually becomes tensile when the film microstructure changes at the high sputtering gas pressure [29, 32].

In 1987, Windischmann [33] developed a model of intrinsic stress for polycrystalline

sputtered film. According to this model, the compressive intrinsic stress in film is produced by an energetic deposition process. The stress is proportional to the product of the flux of energetic grains and the square root of the particle energy as given by Eq. (2. 2).

$$\sigma_{in} = 1.91k\, j\, E_p^{1/2} Q/N_0 \qquad (2.\ 2)$$

Where j is atomic flux, E_p is the projectile energy, Q is the elastic energy per mole, and N_0 is the Avogadro's number. It is clear that stress increases with increasing particle energy.

(2) Recrystallization effect

The recystallization effect is one of the mechanisms accounted for the large tensile intrinsic stress in thin film [28]. Klockholm and Berry [34] reported a model that the stress arises from annealing and shrinkage of disordered material buried below the advancing surface of the growing film. The magnitude of the stress indicates the amount of the disorder present on the surface layer before it is covered by successive condensing layers. If the film is assumed to grow at a steady-state rate of G monolayers/s, the atoms will roughly remain on the surface for a time 1/G. In this time interval, thermally activated atom movements promote recrystallization on the film surface. The rate of this process (r) is described by Eq. (2. 3)

$$r = \upsilon_0 \exp -(E_R/RT_S) \qquad (2.\ 3)$$

Where υ_0 is a vibration frequency factor, E_R is appropriate activation energy, and T_s is the substrate temperature. Basically, high growth stress corresponds to the condition, $G > r$, and low stress to the reverse case.

(3) Island coalescence

The generation of intrinsic stress in film growth by Volmer-Weber model can be explained based on the island coalescence mechanism, developed by Hoffman [21]. In Volmer-Weber film growth model, the islands enlarge during the film deposition. As two neighbor islands grow, they become close enough for adjacent surfaces to experience a force of attraction and snap together. The interatomic forces cause a constrained relaxation of the top layer of each surface when the grain boundary forms. As a result, a stress can be described by Eq. (2.4)

$$\sigma = \frac{E_f \Delta p}{(1-\upsilon) l_g} \qquad (2.4)$$

Where, l_g is the average grain size, Δ is the constrained relaxation length, E_f is Young's modulus, υ is the Poisson ratio, and p is the packing density of the film. The coalescence process gives rise to tensile stress driven by the reduction in interfacial/surface energies, as described by Eq. (2. 5)

$$\Delta\gamma = \gamma_I - 2\gamma_S \qquad (2.5)$$

where γ_I is the free energy of the newly formed grain boundary, and γ_S is the free energy of the solid/vapor surface prior to coalescence. It is noted that $\Delta\gamma$ must be negative for coalescence to be thermodynamically viable [21]. Taking $\Delta\gamma$ instead of Δ and assuming $p = 1$ in Eq. (2. 4), the maximum film stress is then expressed as

$$\sigma_{max} = \left(\frac{-2E_f \Delta\gamma}{(1-\upsilon) l_g}\right)^{1/2} \qquad (2.6)$$

2.1.2 Thermal stress

The thermal stress of thin film is caused from the thermal mismatch between the film and the substrate. This stress component is clearly described as a function of temperature in the Eq. (2. 7) [35]

$$\sigma_{th} = \int_{T_1}^{T_2} \frac{E_f(T)}{1-\nu_f} (\alpha_s - \alpha_f(T)) dT \qquad (2.\ 7)$$

Where $E_f(T)$, $\alpha_f(T)$ and υ_f are Young's modulus, coefficient of thermal expansion (CTE), and passion ratio of the film, respectively. α_s is the CTE of the substrate. The term of $E_f(T) / (1 - \upsilon_f)$ is called the biaxial modulus of the film. Carcia *et al.* [32] reported that the biaxial modulus of ITO is taken equal to 180 GPa. The CTE value of ITO film ranges from 6 ppm/ ℃ to 10 ppm/ ℃ [32, 36, 37]. T_1 and T_2 are the absolute temperatures. Usually, T_1 is the absolute temperatures of film deposition and T_2 is the absolute temperature, at which the stress is measured. Therefore, the thermal stress of thin film equals zero at the deposited temperature.

2.2 Optical properties of ITO films

The wavelength dependence of transmittance and absorption can be used to estimate the optical band gap of materials by Eq. (2. 8)[38]

$$\alpha \propto (h\nu - E_g)^{1/2} \qquad (2.\ 8)$$

Where α is the absorption coefficient, E_g is the optical band gap, and hv is the photon energy. According Eq. (2. 8), the intercept on the hv axis from an extrapolation of the linear region on the plot of α^2 *vs*. hv gives the energy band gap of films [39-41].

ITO is a direct optical band gap material with the band gap generally greater than 3.75 eV, although a range of values from 3.5 to 4.06 eV have also been reported in the literature [42, 43]. The shift in optical band gap can be explained by two following mechanisms:

(1) For the films with moderate carrier concentration, the optical energy band gap increases with increasing carrier concentration, *i.e.* Burstein-Moss (BM) shift, as expressed in Eq. (2. 9)[44]

$$E_g = E_{gi} + \frac{\pi^2 h^2}{2m^*_{VC}}\left(\frac{3N}{\pi}\right)^{2/3} \qquad (2.\ 9)$$

Where E_{gi} is the intrinsic energy gap and m^*_{VC} is the reduced effective mass, given by Eq. (2.10) as reported by Kim *et al.*[39]

$$\frac{1}{m^*_{VC}} = \frac{1}{m^*_V} + \frac{1}{m^*_C} \qquad (2.\ 10)$$

Where m^*_C and m^*_V are effective masses of carriers on conduction and valence bands, respectively. The BM shift increases when low energy levels in the conduction band are filled

up.

(2) For ITO films with significantly high carrier concentration, the phenomenon of band gap narrowing is attributed to the electron-electron and electron-impurity scatterings [45]. The self energies $\hbar\Sigma$ due to these scatterings are counted into the optical band gap shown in Eq. (2.11)

$$E_g = E_{gi} + \frac{\pi^2 h^2}{2m^*_{VC}}\left(\frac{3N}{\pi}\right)^{2/3} + \hbar\Sigma \qquad (2.\ 11)$$

2.3 Effects of the stress on film properties

It is well known that film stress, which is induced as a film is coated on a substrate due to the material properties mismatch, is an inevitable occurrence. Many researchers have studied the stress effects on film properties for years. Their results show that large film stress could lead to film cracking and discohesion in tension, whereas buckling and delamination in compression [46-50]. These phenomena cause a high electrical resistance and a low optical transparency in the coating films [51-53].

Moon *et al.* [52] reported the cracking phenomenon occurs in lithium manganese oxide thin films as a tensile stress of 1000 MPa. That micro-crack caused a harmful effect on the electrical contact between the substrate and the particle. Similar result was also reported by Sujatha *et al.*[53]. Cairns *et al.* [54] have studied the mechanical behavior of ITO film on PET. The results show that cracking occurs in the film as the uniaxial strain exceeds the critical value, causing a significantly electrical resistance increase in the ITO film. The correlation between number of film cracks and resistance increase ΔR was also described by Eq. (2.12)

$$\Delta R = \frac{\rho D^2 L_0 (1-\varepsilon) \sum_{i=1}^{m} (\varepsilon - \varepsilon_{ci})^2}{V} \quad (2.12)$$

where ε is the instantaneous strain, ε_{ci} is the strain at which the ith crack forms, D is the length scale, m is the number of cracks at strain ε, L_0 is the initial gauge length, and V is the volume of the ITO with each crack. Similarly, Heo *et al.*[55] found that the resistance of ITO film on poly(ether sulfones) (PES) increased with increasing bending cycles. In other words, the

resistance of ITO film increased with increasing film stress.

Caircia *et al.*[29] have studied the stress-working pressure dependence of ITO film deposited on the polyester substrate. It was found that the film stress changed from compressive to tensile stress with increasing working pressure. At working pressure of 12 mTorr, ITO film with a near zero stress value yielded the lowest resistivity of 3.2×10^{-4} Ω cm and highest optical transmission above 80% for wavelength greater than 450 nm. Ng *et al.*[56] revealed that the carrier mobility increased (decreaseds) as the film was under tensile (compressive). The optical absorption spectra were also found to shift with film stress. Moreover, Lappalainen *et al.* [51] found that a strong residual compressive stress in the PNZT films on MgO substrates caused ~3% reduction of the unit cell volume and, subsequently reduction in atomic separation with decreasing film thickness. This caused the absorption edge shift to higher photon energies [51]. This result is in good agreement with the report of Chu *et al.* [57]. They found that the film stress caused the valence band warps, resulting in the band gap change.

Chapter 3 Experimental

3.1 Sample preparation

3.1.1 Substrate preparation

(1) Si substrate

In this thesis, double-side polished Si (100) wafers (6 in. in diameter) are used for two purposes:

(i) Si plays a role of a wafer for PET and PI substrates. Initially, a 6 in wafer was cut into a square shape with the size of 5×5 cm^2, which was subsequently spin-coated polymer as substrate. Then, the wafer with polymer substrate was cut into 5×1 cm^2 strips before the deposition of ITO film.

(ii) Si is also employed as a substrate for ITO stress measurement. For this purpose, the Si wafer was cut into 5×1 cm^2 strips, and cleaned by acetone and alcohol. The curvature of the Si substrate was first obtained by a bending beam measurement before the deposition of ITO film.

(2) PET substrate

Firstly, the polyethylene terephthalate (PET) grains, which is produced by Nan Yan Plastic Corporation, were dissolved into the trifluoroacetic acid (TFA) solvent (purity: 99%;

A Johnson Matthey Company) with a weight ratio of 1: 14. Then, the solution was stirred for 2 days at room temperature in order to dissolve PET grains completely. Afterwards, a 3 μm thick PET film was prepared by spin-coating the PET solution onto the Si wafers ($5\times5\ cm^2$) and drying out the TFA solvent in an vacuum oven for 2 hours at 85 ℃. Finally, the PET/Si sample ($5\times5\ cm^2$) was cut to 5 pieces of $5\times1\ cm^2$ strip samples.

The chemical structures of PET and TFA are schematically illustrated in Figure 3.1 and 3.2, respectively.

(3) ODPA-BAPP polyimide substrate[58]

The polyimide was synthesized from 4,4'-oxydiphthalic anhydride (ODPA) and 2,2'-bis[4-(4-aminophenoxy)phenyl]propane (BAPP) developed by Mr. Shao-Nung Huang [58]. The ODPA and BAPP are produced by Sigma Aldrich Co. and Tokyo Chemicals Industry Co., respectively. The N,N-Dimethyl-acetamide (DMAc) (99.5% purity) was used as a solvent. The chemical structurse of dianhydride and diamine starting monomers, and DMAc solvent are schematically shown in Figure 3.3, 3.4, and 3.5, respectively.

In this synthesis, the BAPP powder was first added into the DMAc solvent, and then stirred at room temperature. When the BAPP was dissolved completely in DMAc, the ODPA powder was added into the BAPP solution, and stirred for 2 days to dissolve ODPA and obtain a uniform poly (amic acid) solution with high viscosity. Then, the solution was spun

onto a 5×5 cm^2 Si wafer. The film was subsequently heated in an oven from room temperature to 250 ℃ with a quite complicated heating process as illustrated in Figure 3.6 to form a polyimide film with thickness ~ 3 μm. The chemical structure of ODPA-BAPP polyimide is shown in Figure 3.7.

For stress measurement, the 5×5 cm^2 PI/Si sample was cut into 5×1 cm^2 strips before depositing ITO film.

(4) Substrate preparation for Hall Effect and UV-visible measurements

Polymers, such as PET and PI, with a thickness of 3 μm were spun on 1×1 cm^2 glass plate for Hall Effect and UV-visible measurements.

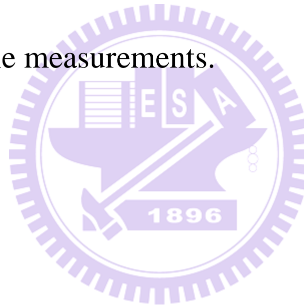
ES A 1896

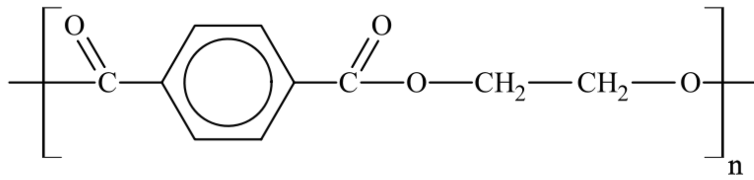

Figure 3. 1 Chemical structure of PET film

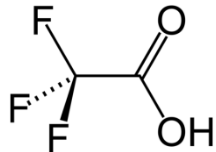

Figure 3. 2 Chemical structure of TFA solvent

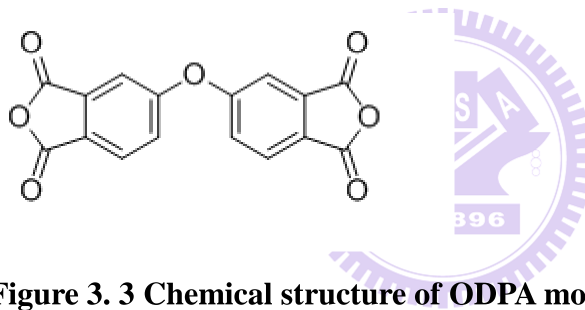

Figure 3. 3 Chemical structure of ODPA monomer

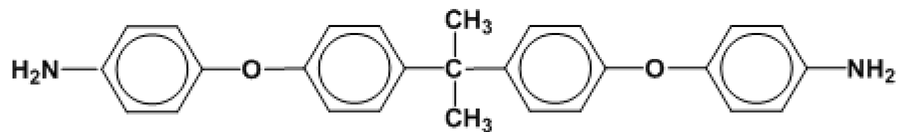

Figure 3. 4 Chemical structure of BAPP monomer

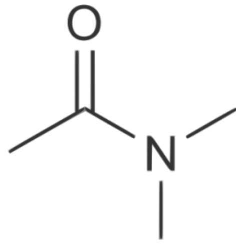

Figure 3. 5 Chemical structure of DMAc solvent

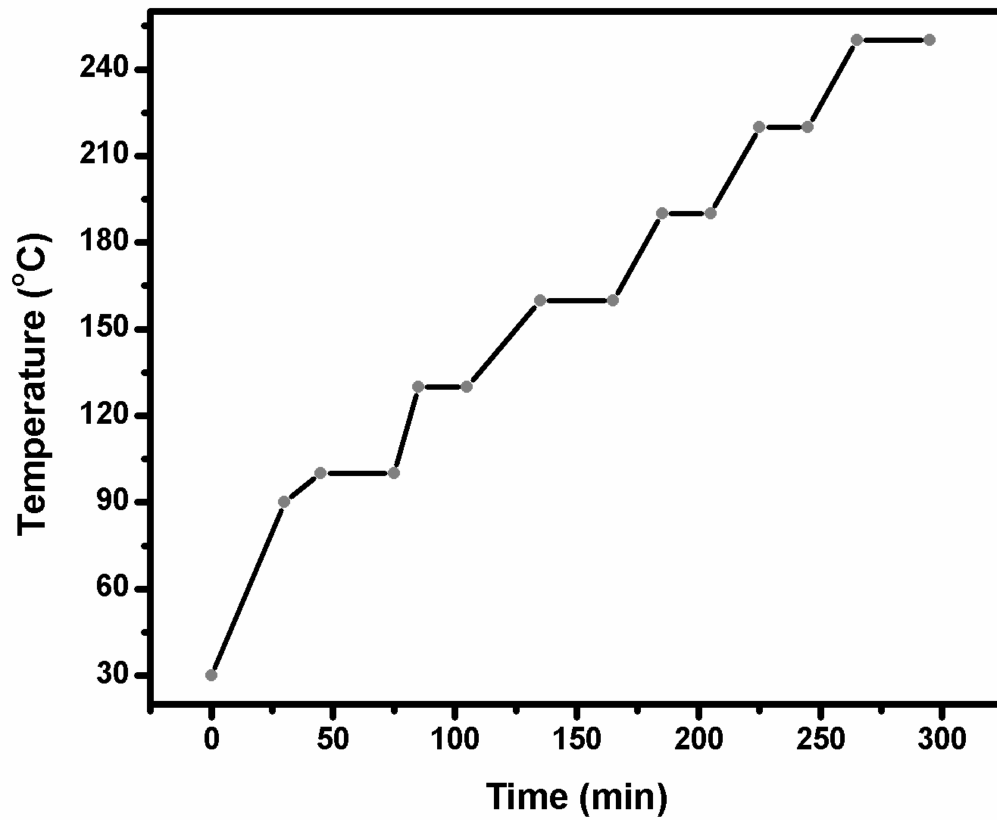

Figure 3. 6 Temperature – time profile for curing of polyimide

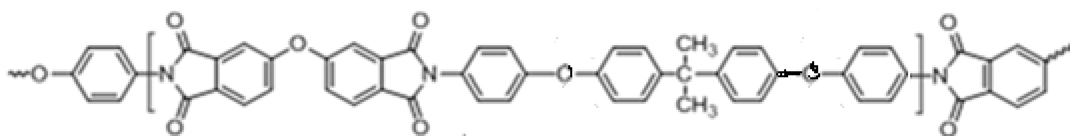

Figure 3. 7 Chemical structure of ODPA-BAPP polyimide film

3.1.2 Indium tin oxide layer deposition

Indium tin oxide (ITO) thin films were deposited at room temperature (RT) and 200 ℃ by a magnetron sputtering system in Paragon Technology Corporation. ITO target (58 cm × 15 cm) is composed of In_2O_3 with 10 wt % SnO_2. The ITO deposition parameters optimized for high conductivity and transmittance are detailed in Table 3.1. The deposition of ITO film was carried out at 1000 W power and 2.74 mTorr working pressure. The gas ambient is oxygen and argon mixture with a ratio of 0.33. The list of samples under different deposition temperature and substrates is summarized in Table 3.2.

Table 3. 1 Condition of ITO film deposition

Target material	ITO (In_2O_3 : SnO_2 = 90.0 : 10.0 Wt%)
Working pressure (mTorr)	2.74
Power (W)	1000
Ar flow rate (sccm)	300
O2 flow rate (sccm)	5
Thickness (nm)	140
Deposited temperature (°C)	RT, 200℃

Table 3. 2 The deposition temperature and substrates for ITO/substrate samples

ITO deposition temperature	Substrates
RT	Si, PET/Si, PI/Si, PET/glass, PI/glass, glass
200 ℃	Si, PI/Si, PI/glass, glass

3.2 Experimental procedures

Figure 3.8 shows the flow chart of experimental procedures. The stress behavior of either polymers substrates or ITO films was measured by a home-built bending beam system. A spectrophotometer was used to measure the UV-visible (UV/Vis) spectra of the ITO films. The electrical properties of ITO films were also investigated by using Hall Effect measurement in this thesis. The morphology of ITO film was studied by a scanning electron microscope (SEM) to obtain the film morphology. The film structure was characterized by using X-ray diffraction (Siemens Diffractometer D8000, Cu Kα, λ=1.5405Å). The details of these analytic instrumentations will be further described in the latter section.

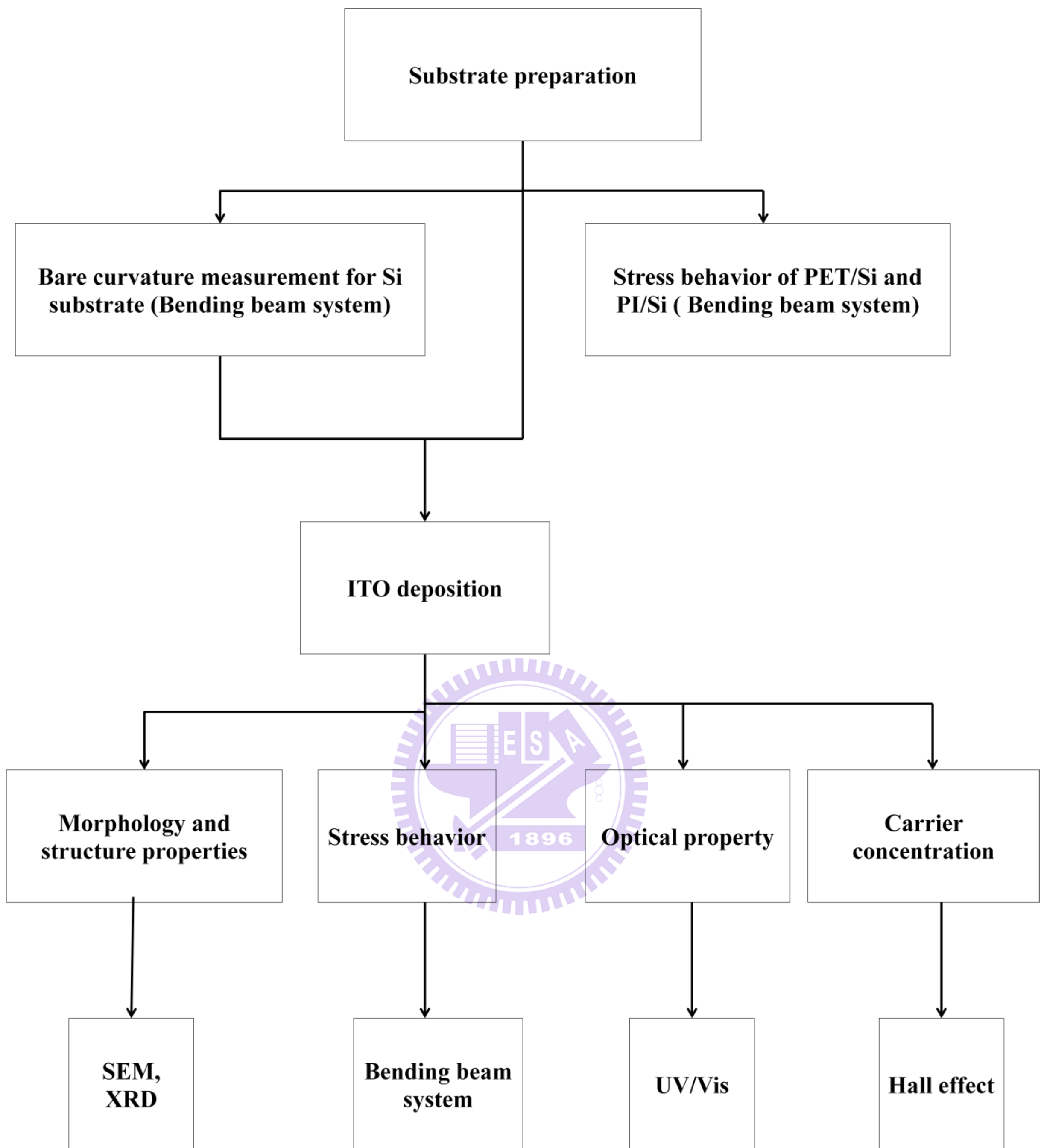

Figure 3. 8 Flow chart of experiment procedures

3.3 Instrumentation

3.3.1 Bending beam system

The stresses of the thin films as a function of temperature were obtained by measuring the radius of curvature of the films on silicon strips using a home-built bending beam system. The measurement bases on the change of the laser light reflection on the sample surface when sample bends due to the stress induced in the coated film. Figure 3.9 details the stress measurement principle. A laser beam from the He-Ne laser source was split into two beams by the beam spitting cube and mirror system before reaching the surface of sample, which is placed inside the vacuum chamber. The sample is required to be mirror-like in order to reflect the two laser beams as they arrive on the sample surface. A double-side polished wafer can serve as a good reflector for this purpose. In the measurement, the sample is heated inside a Cu heating chamber. The directions of two reflected laser beams changed with the change of temperature due to the sample bending. A position sensor system is used to detect the reflected laser beams position. The optical signal is amplified by an amplifier, and then changed into the analog signal, and finally transferred to a computer through data acquisition interface card (national Instruments) and Labview program. Through the integration of computer, data acquisition, and software, the measurement system can record the bending curvature of sample from the distance between two reflected laser spots as a function of thermal cycling as described latter. The stress of a thin coated film based on Stoney's Eq.[59]

can be expressed as Eq. (3.1)

$$\sigma = \frac{E_s\ t_s^2}{6(1-\upsilon_s)t_f}\left[\frac{1}{R} - \frac{1}{R_o}\right] \qquad (3.1)$$

Where, E_s is the Young's modulus of the substrate. υ_s is the Poisson ratio of the substrate, t_s and t_f are the thickness of the substrate and the film, respectively. R is the radius of curvature of the film on the substrate and R_o is the radius of curvature of the bare substrate after the thin film is removed. The term of $(1/R - 1/R_0)$ is so-called the bending curvature of a sample. The Eq. (3.1) assumes that both film and substrate are isotropic and film is much thinner than substrate ($t_f < 0.06\ t_s$)[59].

Figure 3.10 illustrates the principle for obtaining the bending curvature of a sample in the bending beam system. It is considered the sample before bending as a line along the x axis, and y axis is normal to the x axis. Under the lab coordinate, the deflection of the sample during the bending is a function of x: y = f(x). When the dy/dx is small, then the sample bending curvature is related to the second derivative [60]

$$\frac{1}{R} - \frac{1}{R_o} = -\frac{d^2y}{dx^2} \qquad (3.2)$$

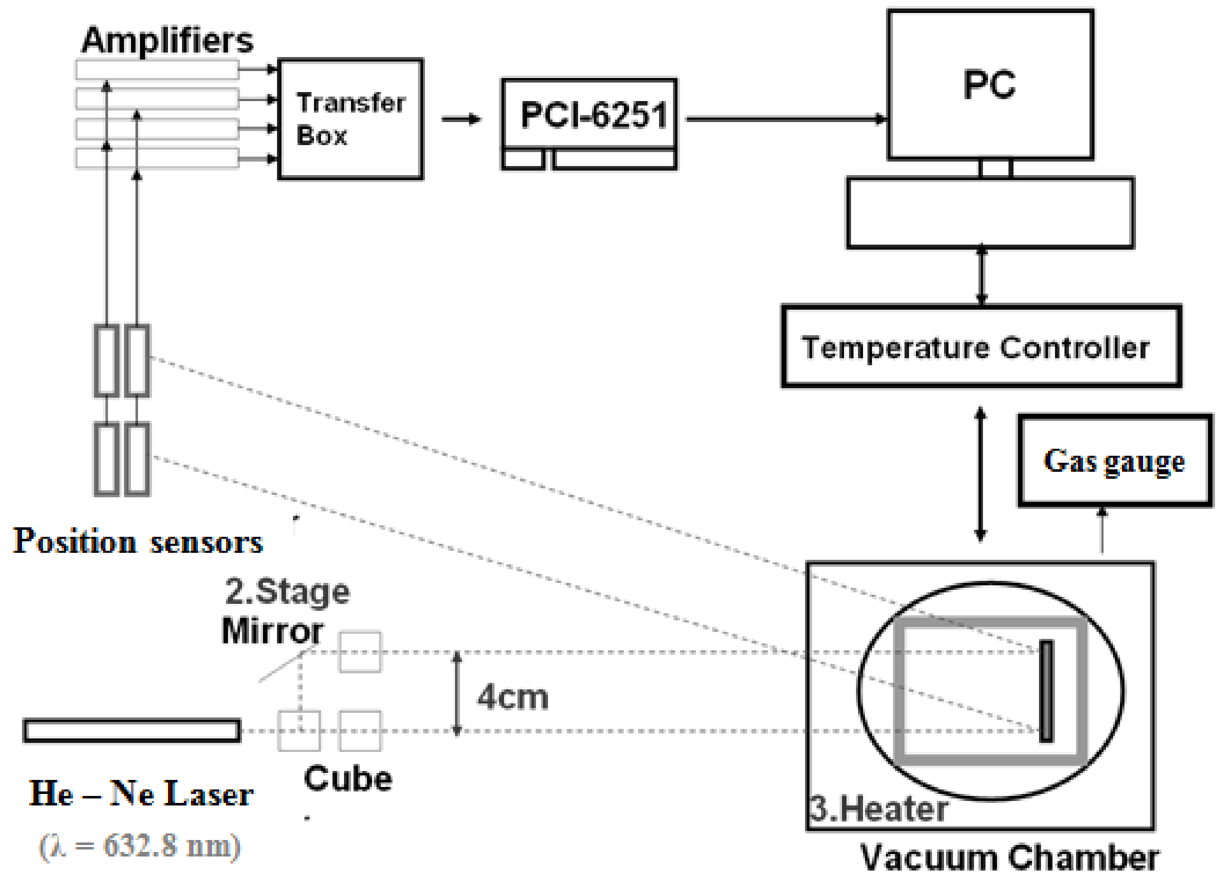

Figure 3. 9 Schematic diagram of a bending beam system

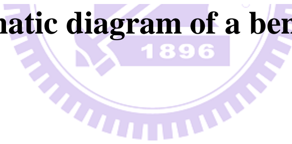

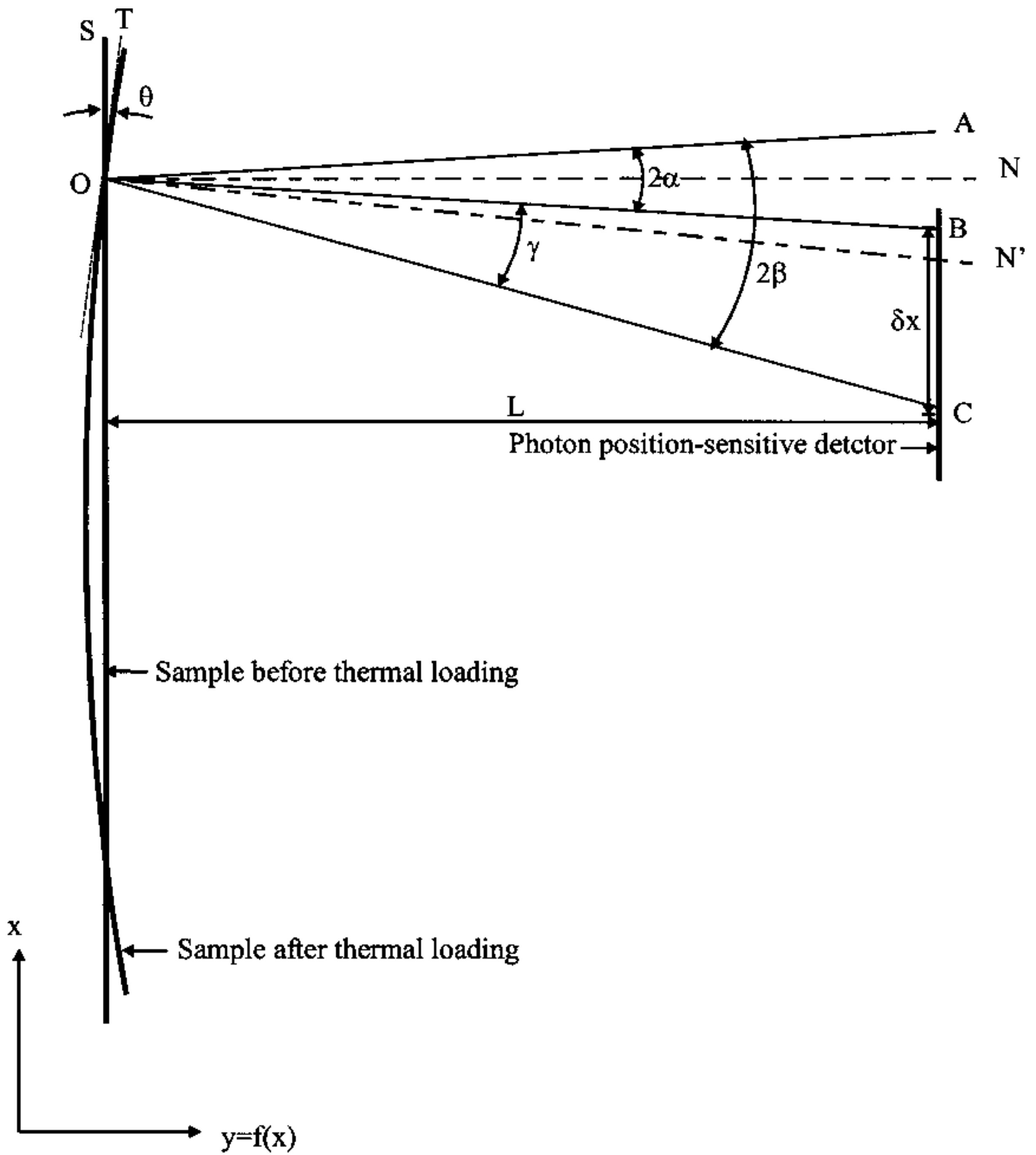

Figure 3. 10 Principle for determining the bending curvature of sample [60]

In Figure 3.10, AO is the incident laser beam. ON and ON' are normal to the sample surface before and during thermal loading. TO is the tangent line of the curve at the laser incident point and OB and OC are reflected beams from the sample before and during thermal loading. From the geometry, it is clear that:

$$\gamma = 2\beta - 2\alpha \qquad (3.3)$$

$$\theta = \beta - \alpha \qquad (3.4)$$

Thus

$$\theta = \frac{1}{2}\gamma \qquad (3.5)$$

ESA 1896

When the incident angle α and the deformation of the package θ are small:

$$\left(\frac{dy}{dx}\right)_{x=x_0} = \tan\theta \approx \theta = \frac{1}{2}\gamma \approx \frac{\delta x}{2L} \qquad (3.6)$$

Where L is the optical path and δx is the displacement of the reflected laser spot on a photon position-sensitive detector during thermal loading. By using two laser beams and two detectors, dy/dx can be measured at two different points, x_1 and x_2. When $D = x_2 - x_1$ is relatively small compared with the radius of curvature of the line, the second derivative can be calculated by Eq. (3.7)

$$\frac{d^2y}{dx^2} \approx \frac{\left.\frac{dy}{dx}\right|_{x_2} - \left.\frac{dy}{dx}\right|_{x_1}}{x_2 - x_1} \qquad (3.7)$$

Combining Eq.s (3.6) and (3.7), the bending curvature is expressed as below:

$$\frac{1}{R}-\frac{1}{R_0}=-\frac{d^2y}{dx^2}=\frac{\delta x_1-\delta x_2}{2DL}=\frac{S_0-S}{2DL} \qquad (3.8)$$

Where S is the distance between two laser spots on position sensor as the substrate is with film, S_0 is the distance between two laser spots on position sensor as the substrate without film (See Figure 3.11).

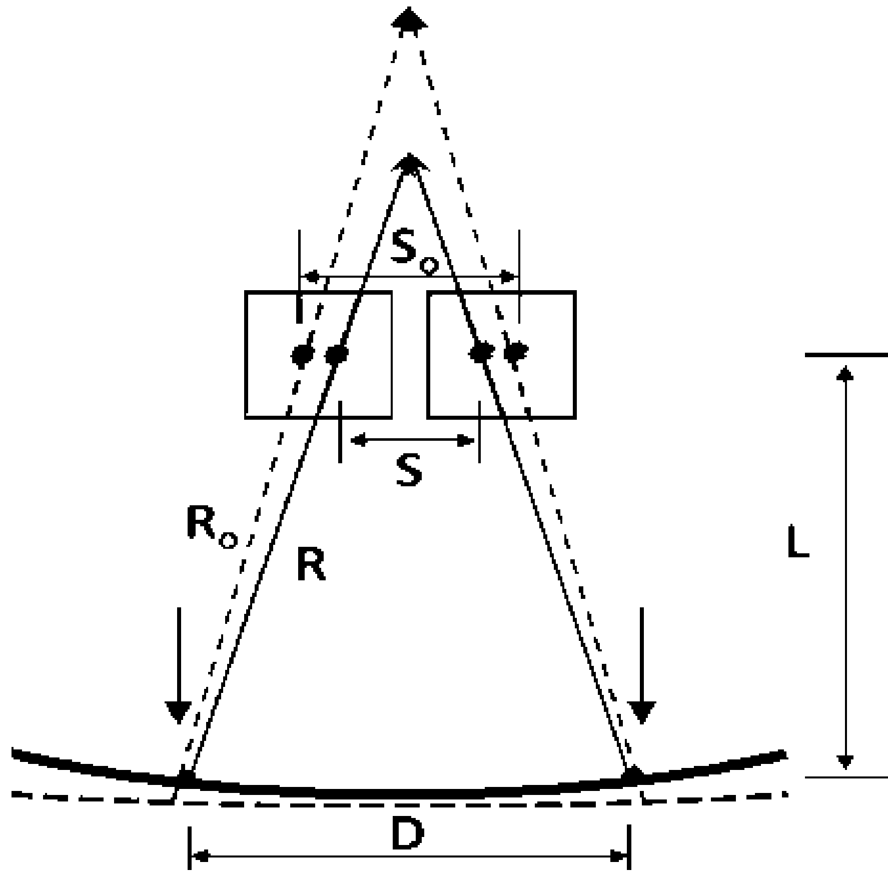

Figure 3. 11 Spatial relationship among parameters in Eq. (3.8)

In the present work, for the samples ITO/Si, the distances S_0 were measured before the ITO film deposition. Then, the distances S were obtained after coating ITO on substrate. However, for cases of polymer substrates, the S_0 were also determined with Si wafer. The stress sample size is only (5 cm × 1cm) however the spin-coating of the polymers requires a square wafer. Therefore, the distances S were first determined after depositing ITO film on polymer (PI or PET)/Si substrate. Then, the film and polymer (PI or PET) were taken out the Si wafer. Subsequently, the S_0 were verified. The distance between two incident laser beams, D, equals to 4 cm. The optical path, L, is 2 m long.

3.3.2 Scanning electron microscope

The morphology of ITO film was examined by a scanning electron microscope (SEM) HITACHI – S2500 JSM – 6700.

SEM is a type of electron microscope that uses the high energy beam to image the sample surface. The electron react with atoms in sample surface and products the information of surface sample topography[61]. In a typical SEM shown in Figure 3.12, an electron beam is thermionically emitted from an electron gun fitted with a tungsten filament cathode[62]. The electron beam, which typically has an energy ranging from 0.5 KeV to 40 KeV, is focused by one or two condenser lenses to a spot about 0.4 nm to 5 nm in diameter. The beam passes through pairs of scanning coils or pairs of deflector plates in the electron column, typically in the final lens, which deflect the beam in the x and y axes so that it scans in

a raster fashion over a rectangular area of the sample surface.

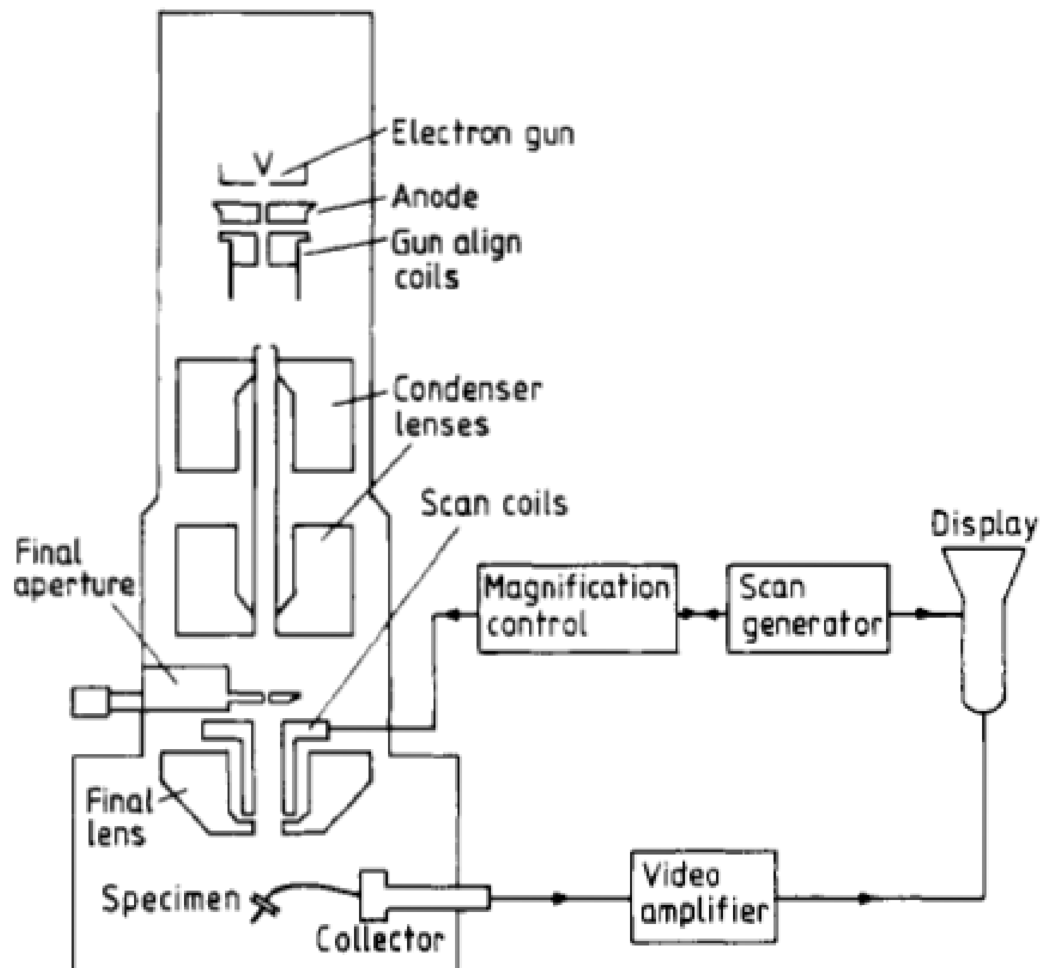

Figure 3. 12 Schematic diagram of an SEM

3.3.3 X-ray diffraction

X-ray diffraction (XRD) is a non-destructive tool for analyzing material properties such as crystallinity, the phase identification, and orientation.

XRD was utilized to analyze the crystallinity in this study. The samples were scanned from 20 degree to 60 degree by Siemens Diffractometer D8000 with small angle ~ 3 degree and step size ~ 0.02 degree. The Xray source is used in the system is Cu Kα (λ=1.5405Å). During scanning period, X-ray beam of wavelength λ was irradiated to the sample at an angle θ, and the diffracted intensity at an angle 2θ was recorded by a detector as illustrated in Figure 3.13.

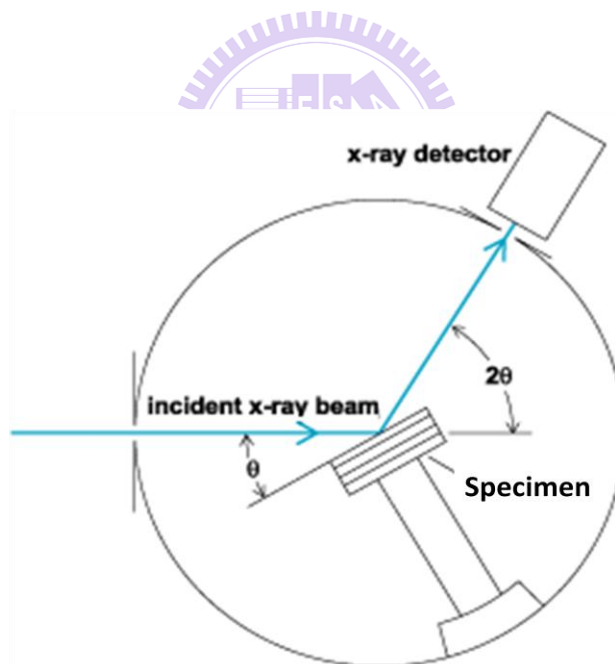

Figure 3. 13 Definition of the angle of incidence and diffraction in an XRD experiment

3.3.4 Hall Effect measurement

Hall Effect refers to potential difference (Hall voltage) on opposite sides of a thin sheet of conduction or semiconducting materials through, which an electric current of flowing, created by a magnetic field applied perpendicular to the Hall element.

From the Hall Effect measurements, the following electrical properties of material can be obtained

(1) The sheet resistance, from which the resistivity can be determined for a sample with a given thickness.

(2) The sheet carrier density of the majority carrier (the number of majority carriers per unit volume). The density of semiconductor (doping level) can be found for a sample with a given thickness.

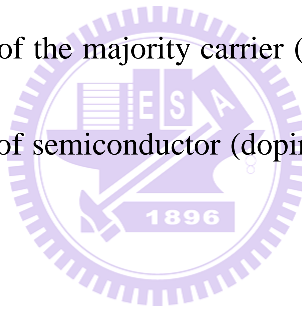

(3) The mobility of the majority carrier.

(4) The doping type of material.

Taking measurements

(1) Current I_{AB} is a positive DC current measured in amperes

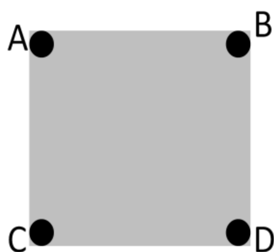

(i) Injected into contact A

(ii) Take out of contact B

(2) Voltage V_{DC} is DC voltage (V)

Measure between contacts C and D with no externally applied magnetic filed

(3) Sheet resistance Rs is measured in Ohms (Ω) by applied the Ohm's law shown in Eq. (3.9)

$$R_{AB,CD} = V_{CD} / I_{AB} \quad (3.9)$$

Taking several reciprocal measurements and averaging to get more precise results.

In this study, the carrier concentration of ITO on PET and ITO on PI samples were obtained by employing a Van der Pauw technique Bio-Rad Micro-science HL 5500 PC. The voltage between contacts C and D, V_{CD}, was 20 mV.

3.3.5 UV-visible spectrophotometer system

An analytical technique for the measurement of wavelength-dependent attenuation of ultraviolet, visible and near-infrared light and used in the detection, identification and quantification of atomic and molecular species. A UV/VIS spectrophotometry V670 (JASCO Corporation) was used to determine the absorption or transmission of UV/VIS light (180 to 900 nm) by a sample. It could also be used to measure concentrations of absorbing materials based on developed calibration curves of the material. Ultraviolet-visible (UV-vis) spectra of the polymer films were recorded on a HP G1103A spectrophotometer.

Chapter 4 Results and discussion

4.1 Thermo-mechanical parameters of ITO film and substrates

The thermo-mechanical parameters of ITO films and substrates were listed in Table 4.1. The coefficient of thermal expansion of ITO films of thickness ~ 140 nm is about 8-11 ppm/℃[63]. The Young's modulus and Poisson ratio of ITO film are 200 GPa and 0.35, respectively [63]. It is revealed that among Si, PET and ODPA-BAPP polyimide substrates, Si is the most rigid substrate with the Young's modulus of 131 GPa[25]. The Young's modulus of PET substrate is 3.5 GPa[63], compared to that of polyimide, 5.6 GPa, which was tested by nanoidentation technique (MTS Nano Indentor XP)[64]. This indicates the PET is softer than Si and polyimide. The CTE of Si, PET and ODPA-BAPP polyimide are 2.61 ppm/℃[25], 50 ppm/℃[64] and 40 ppm/℃[64], respectively, and their Poisson ratios are 0.278[25], 0.44[63] and 0.34[65]. Table 4.1 also shows the glass transition temperature (T_g) values of PET and ODPA-BAPP polyimide. T_g of PET is very low, 70-80 ℃, compared with 230 ℃[58] of PI film.

Table 4. 1 Thermo-mechanical properties of ITO film and various substrates

Materials	Thickness (μm)	CTE (ppm/^{0} C)	Modulus (GPa)	Poisson ratio	T_g (℃)
Si[25]	525	2.61	131	0.278	-
PET	3.5	50[64]	3.5[63]	0.44[63]	70-80
PI	3.5	40[64]	5.6	0.34[65]	230
ITO[63]	0.14	8-11	200	0.35	-

4.2 Stress behavior of ITO film deposited on Si substrate

This section describes the stress behavior of ITO films deposited at both room temperature and 200 ℃ on Si substrate. The ITO film thickness is 140 nm. The film stress was measured in 2-3 thermal cycles within 30 – 200 ℃ in 45 Torr nitrogen ambient. The samples were heated with a rate of 2 ℃/min up to 200 ℃, and then naturally cooled.

4.2.1 Stress of ITO film deposited at room temperature on Si substrate

Stress behavior of room – temperature deposited ITO film was first investigated. From Figure 4.1, it is observed that indium tin oxide film on silicon substrate exhibits a tensile stress in a range of 80-330 MPa. The stress-temperature curve starts with the initial stress value of 185 MPa. The stress of thin film includes two components, intrinsic stress and thermal stress. The intrinsic stress is generated from the materials mismatch between film and substrate during the film deposition. The thermal stress, which is a function of temperature given by Eq. (4.1), is caused by the difference in thermal expansion between the film and the substrate. Since the indium tin oxide film has higher coefficient of thermal expansion than Si substrate, the film thermal stress becomes compressive with increasing temperature. Therefore, the film residual stress decreases during the heating process.

$$\sigma_{th} = \frac{E_f}{1-\upsilon_f}(\alpha_s - \alpha_f)(T - T_d) \qquad (4.1)$$

Where, E_f, α_f, and υ_f are Young's modulus, coefficient of thermal expansion (CTE), and possion ratio of the film, respectively. α_s is the CTE of the substrate. T is the temperature, at

which the film stress is recorded. T_d is the deposition temperature.

The stresses at room temperature of ITO film after the first and the second thermal cycles are 310 MPa and 330 MPa, respectively. It means that the film stress is relieved cycle-by-cycle (-125 MPa in the first cycle and -20 MPa in the second cycle). This result indicates the film structure is getting stable after thermal cycles. The stress of ITO film at room temperature after two thermal cycles is 330 MPa. The total relief stress of the film after two thermal cycles is – 250 MPa.

It is noted that the stress-temperature curve of ITO film on Si is non-linear indicating the film residual stress is not only thermal in origin. The non-linear of stress-temperature curve may result from the film volume shrinkage due to the increase of film particle size during the heating process. As seen from the SEM images in Figure 4.2, the particle size of ITO film increased from 16.5 nm to 19.6 nm after the first cycle, then its size grew up to 20.9 nm when the curing process finished. Therefore, the film tends to shrink but it is stuck well on substrate resulting in the increase of film intrinsic stress after thermal heating.

Figure 4.1 shows that the stress-temperature curve of ITO film starts from a positive stress value revealing the film initial stress is tensile. Generally, the film initial stress comes from two factors, intrinsic stress and thermal stress [19, 23, 66, 67]. The thermal stress results from the thermal expansion difference between the film and substrate when sample temperature differs from deposited temperature as expressed in Eq. 4.1. In this case, the ITO

films were formed at room temperature. Thus, the film thermal stress can be ignored at room temperature. Thus, the intrinsic stress of the ITO film should be equal to the film initial stress, which is tensile as seen in Figure 4.1. It is well known that the intrinsic stress of a sputtered film is commonly compressive due to the atomic peening effect [29]. However, the intrinsic stress of this ITO film may also be attributed to a tensile stress component. The generation of this stress component is still not clearly understood.

The surface morphology of ITO film was tested before and after stress measurement by an optical microscope (OM). Figure 4.3 shows that the surface of the film after thermal cycling is the same as the as-deposited film. That reveals the stress measurement within 30 – 200 ℃ does not cause any damage on the film.

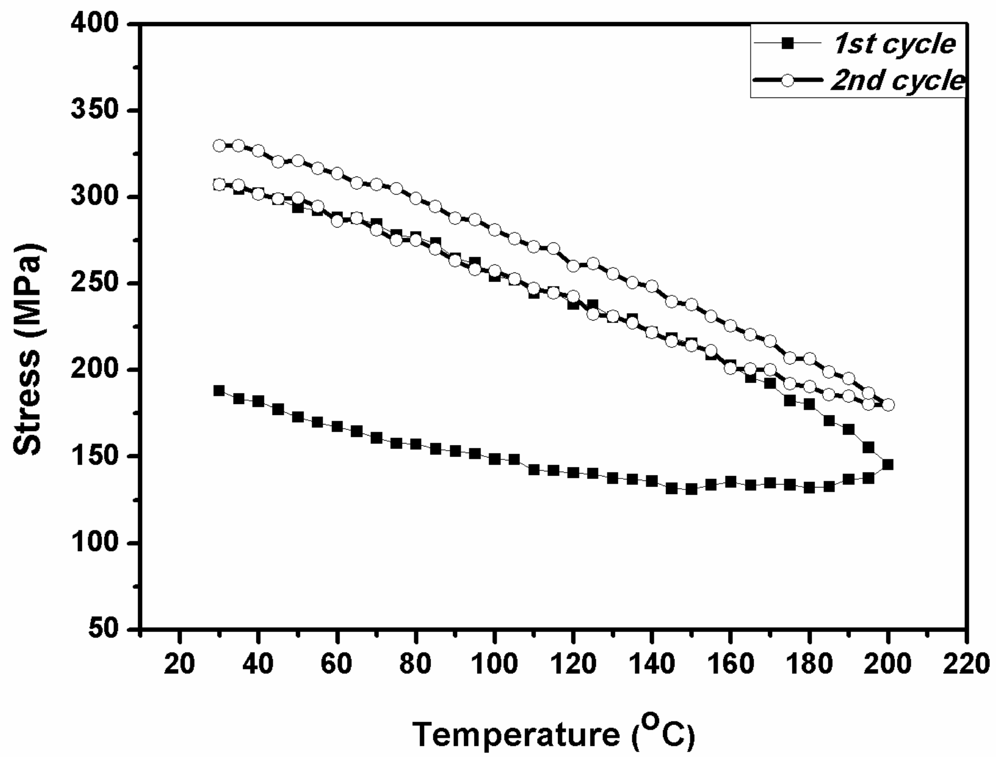

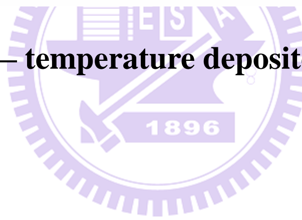

Figure 4. 1 Stress of room – temperature deposited ITO film on Si substrate

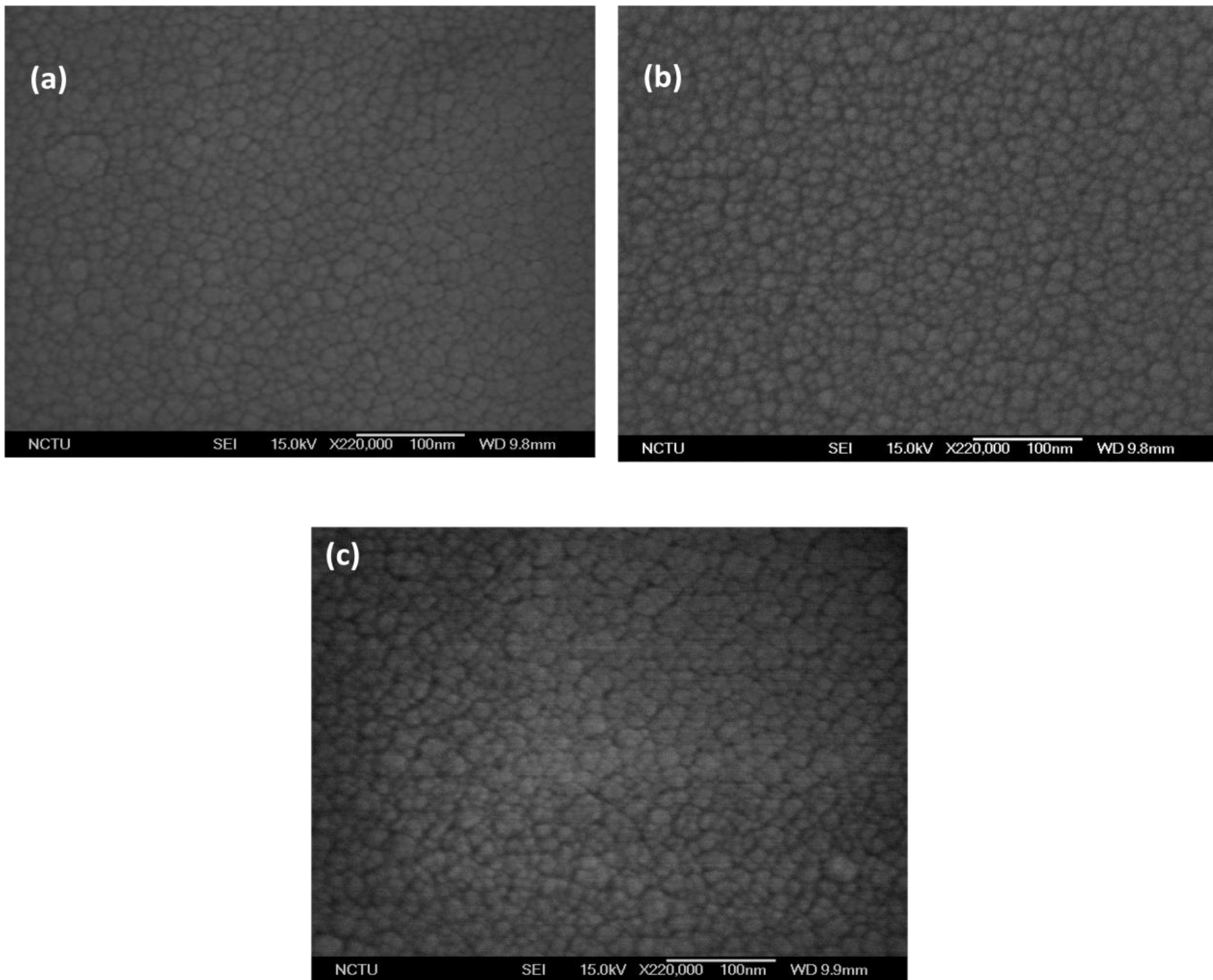

Figure 4. 2 The SEM top-view images of ITO films (a) as-deposited, (b) after the 1st thermal cycle, and (c) after the 2nd thermal cycle

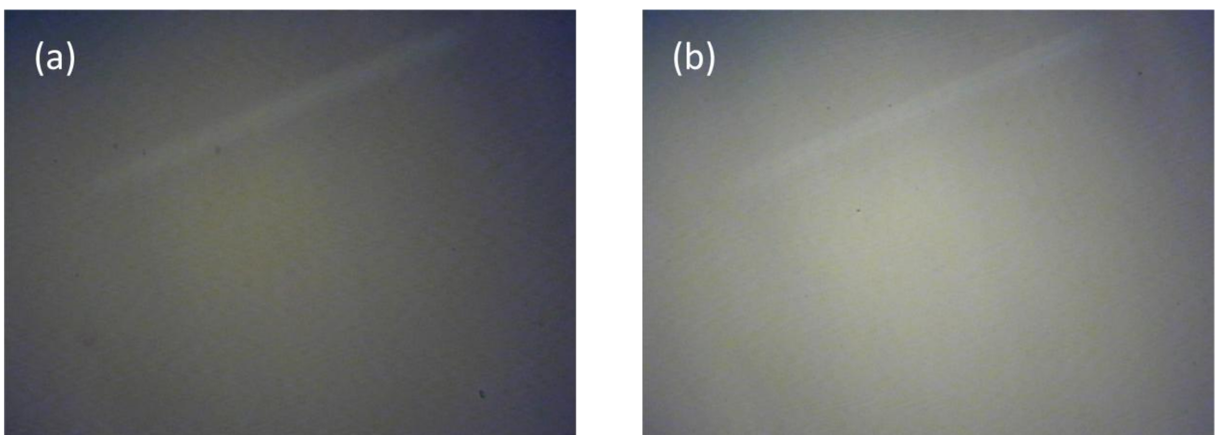

Figure 4. 3 The morphology of (a) as-deposited ITO film and (b) post-deposited ITO film

4.2.2 Stress of ITO film deposited at 200 ℃ on Si substrate

The indium tin oxide films, which are deposited at low temperature (room temperature), are usually amorphous and poor in electrical and optical properties [68, 69]. There are some methods to improve these ITO properties, such as increasing deposition temperature, annealing or other treatments after the deposition [68-71]. Here, the ITO films were deposited at high temperature, 200 ℃. The stress measurement was carried out with three thermal cycles from room temperature to 200 ℃. The result is shown in Figure 4.4.

It is observed that the residual stress of ITO film is in range of -100-200 MPa. The film initial stress is tensile with value of 75 MPa. When the temperature is increased, the residual stress decreases and tends to more compressive. This reveals the stress curve slope is negative, i.e. $[E_f/(1-\nu_f)](\alpha_s-\alpha_f) < 0$. Thus, it can be predicted that coefficient of thermal expansion of ITO film deposited at 200℃ is still higher than that of silicon.

In the first thermal cycling, the ITO film residual stress decreases with increasing temperature. It reaches the zero-stress point at 100℃, then the stress continues developing in the compressive side. The film stress curve achieves a value of -100 MPa at the end of the first heating process. This stress value is thought to be film intrinsic stress because the film was deposited at 200 ℃, which equals to the sample temperature at the end of the heating processes [19]. Compared to the stress behavior of the room temperature deposited ITO film (Table 4.2), stress values of 200 ℃ deposited film are about 100 MPa lower. Specifically, the

intrinsic stress of the high temperature sputtered ITO film is compressive (i.e. negative value, - 100MPa). The compressive tendency of ITO film stress with increasing deposition temperature can be explained by two reasons. The first reason is the increase of particle penning effect, which is caused from the particle bombardment on the growing film surface. The intrinsic stress of a sputtered film depends on the particle energy as mentioned in Chapter 2 and described in Eq. (4.2)[33]

$$\sigma_{in} = 1.91k\, j\, E_p{}^{1/2} Q/N_0 \qquad (4.2)$$

Where j is atomic flux, E_p is the grains energy, Q is the elastic energy per mole, and N_0 is the Avogadro's number. The grains energy is contributed to the total particle thermal energy, which is proportional to the absolute temperature (See Eq. 4.3).

$$E_{th} = N \frac{1}{2} fkT \qquad (4.3)$$

Where E_{th} is the total thermal energy of particle system, N is the number of ITO film grains; f is the quadratic degree of freedom, k is the Boltzmann constant, and T is the absolute temperature of the system. T = 303 K as film is deposited at room temperature while T = 473 K as film is formed at 200 ℃. It means the total thermal energy of ITO grains is increased 1.6 times when the substrate temperature is raised from 30 ℃ to 200 ℃. That leads to an increase of ITO total energy, and then results in the more compressive intrinsic stress. Another reason of compressive stress tendency comes from the improvement of film crystallinity. As illustrated in Figure 4.5, the XRD pattern of ITO film shows that ITO films were deposited at

both room temperature and 200 ℃ are polycrystalline. However, the crystallinity of the film, which was deposited at 200 ℃, is higher than the room – temperature deposited film. That means the ITO film deposited at higher temperature possesses the larger grain. It is believed that those grains sit more closely (it can be seen clearly in the section of polyimide substrate) leading to the stronger inter-grains force. Hence, the intrinsic film stress tends to compressive. Through three thermal cycles, the compressive intrinsic stress is reduced, and the nearly zero-stress is reached in the third thermal cycle.

During the cooling processes, the residual stress tends to tensile stress caused by the development of the film thermal stress. The microstructure change of ITO film makes the stress relieve cycle by cycle and completely relieve after the third cycle, when the film structure achieves a stable state. Film stress at room temperature after thermal cycling is 200 MPa.

The optical microscope (OM) images of ITO film surface after and before stress measurement, which are shown in Figure 4.6, do not pose any cracking or delamination in the film. It means the film morphology was not damaged in the stress range of -100-200 MPa.

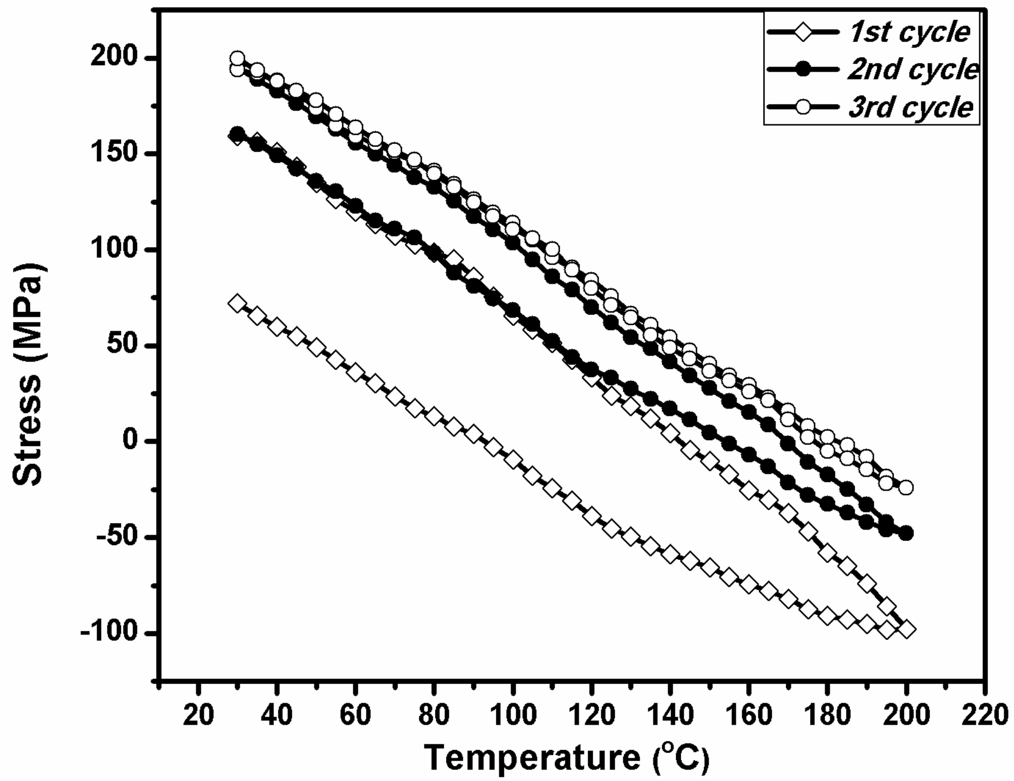

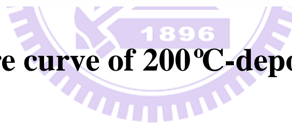

Figure 4. 4 Stress-temperature curve of 200℃-deposited ITO film on Si substrate

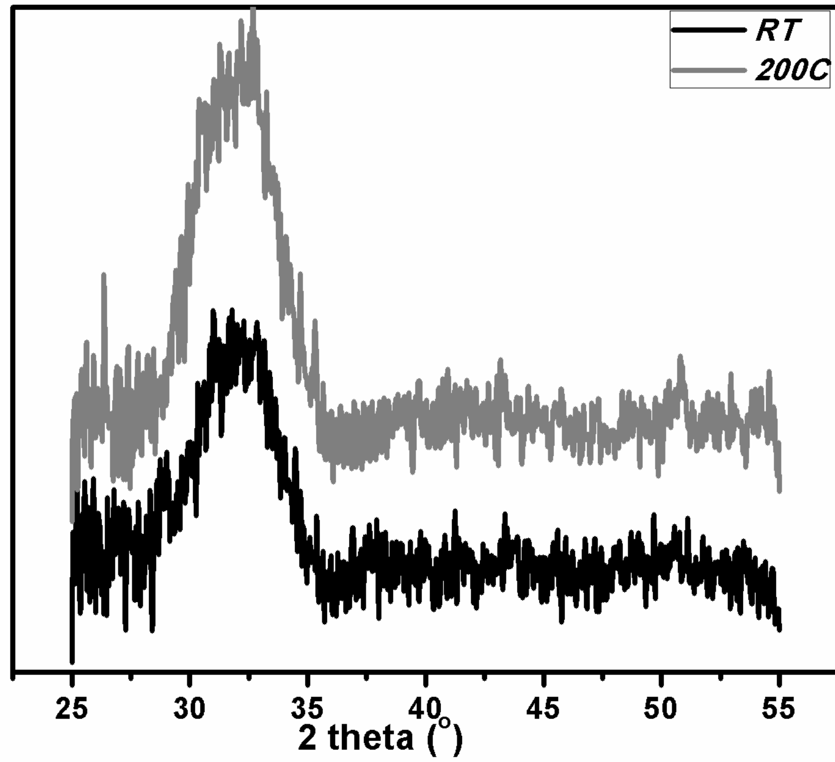

Figure 4. 5 XRD patterns of ITO film deposited on Si substrate at room temperature and 200 ℃

Table 4. 2 The stress comparison for the ITO films deposited at room temperature and 200℃

Td	Stress range (MPa)	Initial stress (MPa)	Intrinsic stress (MPa)	Stress at RT (MPa)	Curve slope (MPa/℃)
RT	80 - 330	185	185	330	- 0.885
200℃	-100 - 200	75	-100	200	- 1.376

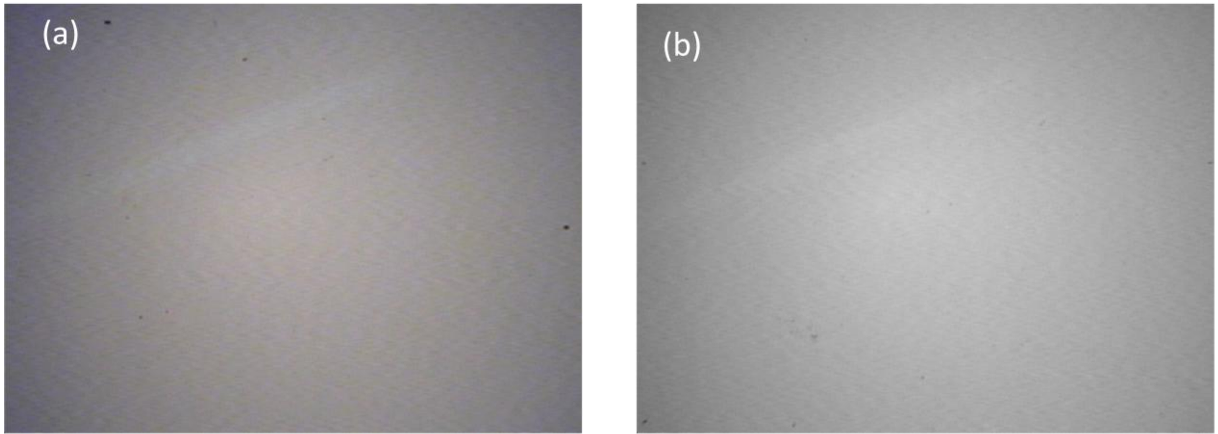

Figure 4. 6 Surface morphology of ITO/Si sample (a) as-deposited and (b) after thermal cycling

4.3 Stress of ITO film on ODPA-BAPP polyimide substrate

Nowadays, polyimide materials receive a lot of attentions in field of flexible devices due to its high flexibility, light weigh, and low cost. They are becoming the best candidates as the substrate of those flexible devices. In the present work, the 4,4'-oxydiphthalic anhydride (ODPA) - 2,2'-bis[4-(4-aminophenoxy)phenyl]propane (ODPA-BAPP) polyimide, which was synthesized by Mr. Shao-Nung Huang[58], is employed as a substrate. The ODPA-BAPP polyimide has high glass transition temperature of 230 ℃. Thus, ITO film is allowed to deposit at high temperature of 200 ℃ on ODPA-BAPP polyimide substrate. In this section, the stress behavior of ITO films, which were formed at both room temperature and 200 ℃ on PI substrate are studied. First of all, the stress behavior of polyimide film on silicon was investigated to aid the stress analysis of ITO/PI layered structure.

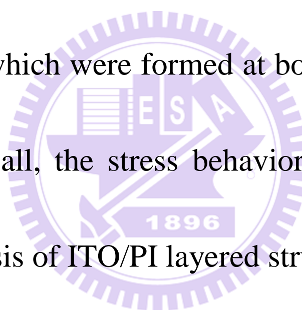

4.3.1 Stress behavior of ODPA-BAPP polyimide film on silicon substrate

The stress measurement of ODPA-BAPP polyimide (PI) on silicon was taken place with the same conditions as those of ITO films on Si and PI substrates. The stress of the PI film on Si as a function of temperature is shown in Figure 4.7.

It is observed that ODPA-BAPP polyimide film on Si is under a tensile stress, i.e. positive stress value, in the range of 5-52 MPa within 30-200℃. The polyimide film was initially stretched on the Si substrate with stress of 52 MPa at room temperature. Since the

ODPA-BAPP polyimide has higher coefficient of thermal expansion than silicon, PI expands more than Si with increasing temperature, resulting in a compressive stress. Thus, the thermal stress develops with increasing temperature, leading to a decrease in the film residual stress. The stress of the ODPA-BAPP polyimide reaches 5 MPa at 200°C. Then the stress increases linearly with decreasing temperature during the cooling cycle and achieves 52 MPa at room temperature. It is clear that the stress behavior along temperature in the second thermal cycle is the same as that in the first one. That indicates the polyimide film is in a stable state, whose stress is completely relaxed after the curing process.

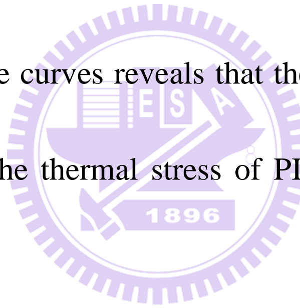

The linear stress-temperature curves reveals that the stress of polyimide film shown in Figure 4.7 is thermal in origin. The thermal stress of PI film is about – 43 MPa, which is calculated by applying Eq. (4. 1).

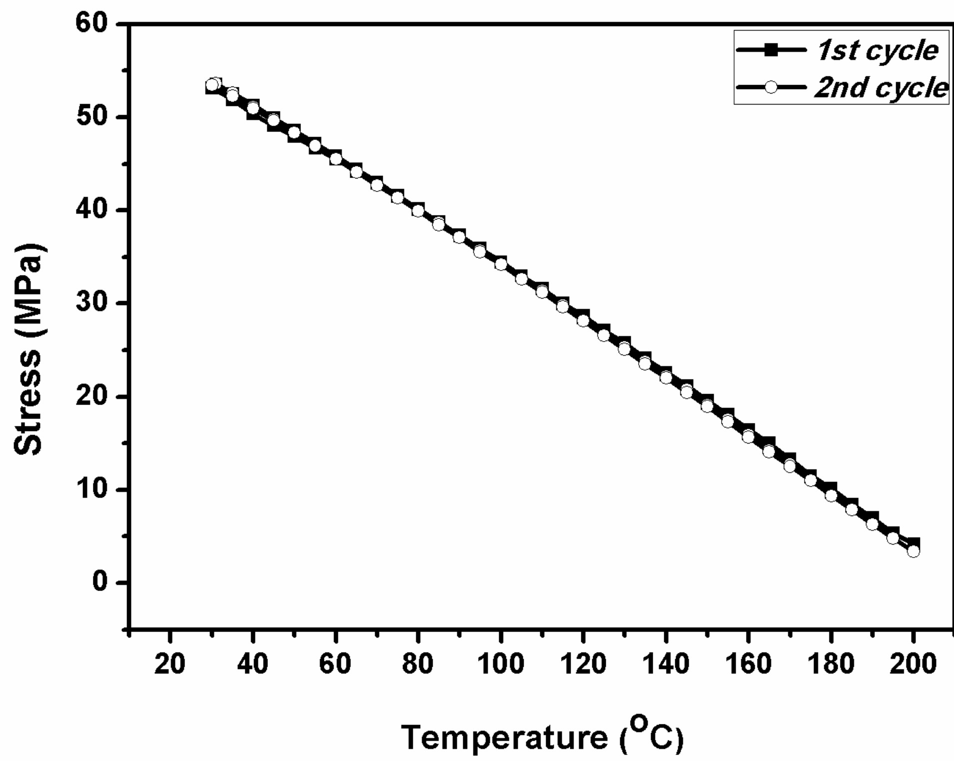

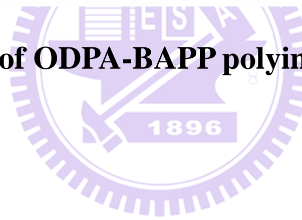

Figure 4. 7 Stress behavior of ODPA-BAPP polyimide film on silicon substrate

4.3.2 Stress of ITO film deposited at room temperature on polyimide substrate

The residual stress vs. temperature for a ITO film on 3-μm ODPA-BAPP polyimide substrate was studied and shown in Figure 4.8 using two thermal cycles. The stress includes of thermal stress and intrinsic stress, ranging in 5 - 71 MPa (i.e. tensile stress) with the initial stress of 55 MPa. As the temperature increases, the compressive thermal stress develops due to the thermal mismatch between ITO/PI and silicon, resulting in a reduction of residual stress. When the sample is heated up to 200℃, film stress reaches to the lowest value of 5 MPa. Subsequently, a tensile stress is induced linearly in the ITO/PI during the first cooling period from 200 ℃ to room temperature with a slope of -0.384 MPa/℃. During the heating cycle, ITO atoms rearrange on PI substrate lead to relieve stress about -16 MPa.

In the both second heating and cooling processes, the stress-temperature curves repeat exactly the first cooling period. It means the ITO/PI has reached a stable state after the first thermal cycle. The film residual stress after that is thermal origin[72]. After two thermal cycles, the residual stress of the ITO/PI attains 71 MPa at 30℃.

A stress hysteresis appears in the first curing cycle and starts decreasing when the sample temperature is higher than 80℃. Furthermore, there is no any stress hysteresis during the second thermal cycle. In contrast, the stress-temperature curve of ODPA-BAPP polyimide film on Si substrate shown in Figure 4.7 does not show any stress hysteresis. Moreover, the

XRD patterns of ITO films before and after stress measurement, which are shown in Figure 4.9, point out that the post-deposited ITO film has higher re-crystalinity than as-deposited film. It means ITO film is crystallized during the thermal cycling, resulting in the film volume reduction tendency. However, the film is cramped on substrate with constant volume. Thus, the crystallinity improvement of ITO film leads the film stress to be more tensile and generate a hysteresis extent in stress vs. temperature curve.

Figure 4.10 shows the OM images of ITO film before and after stress measurement. It is observed that the film surface was not damaged after the thermal cycling.

It is seen from Figures 4.7 and 4.8 that the stress values of ITO/PI are 0 – 20 MPa higher than those of PI film indicating ITO film on ODPA-BAPP polyimide stands a tensile stress, or in other words, ITO film is stretched on PI substrate. Compared to the case of ITO/Si sample, stress values of ITO/PI/Si are 76 % lower. Similarly, Chen *et al.*[72] found that the stress of Cu on fused quartz was reduced 25% with the existent of a polyimide layer between the Cu film and the quartz substrate due to the plastic deformation in the Cu/PI interface. In our case, the plastic deformation is also expected to occur through the interface of the ITO and ODPA-BAPP polyimide. We can demonstrate that the ODPA-BAPP polyimide with high flexibility (low Young's modulus ~ 5.6 GPa) plays a role as a buffer layer in the system of ITO/PI/Si.

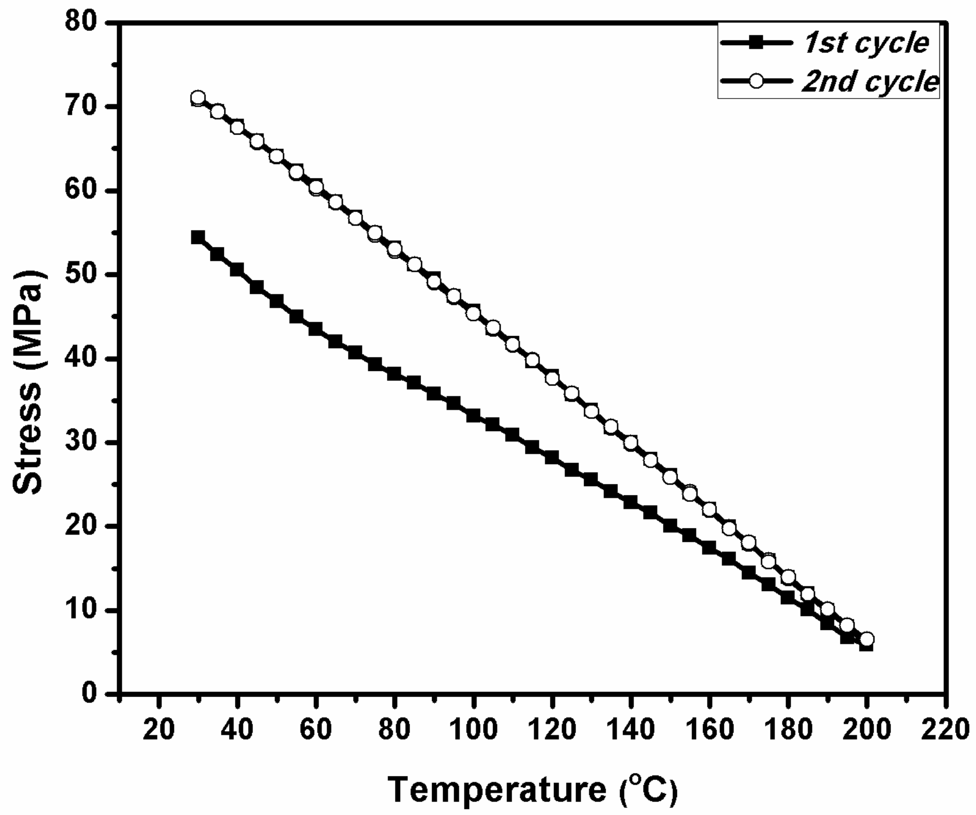

Figure 4. 8 Stress vs. temperature of ITO film deposited at room temperature onto ODPA-BAPP polyimide

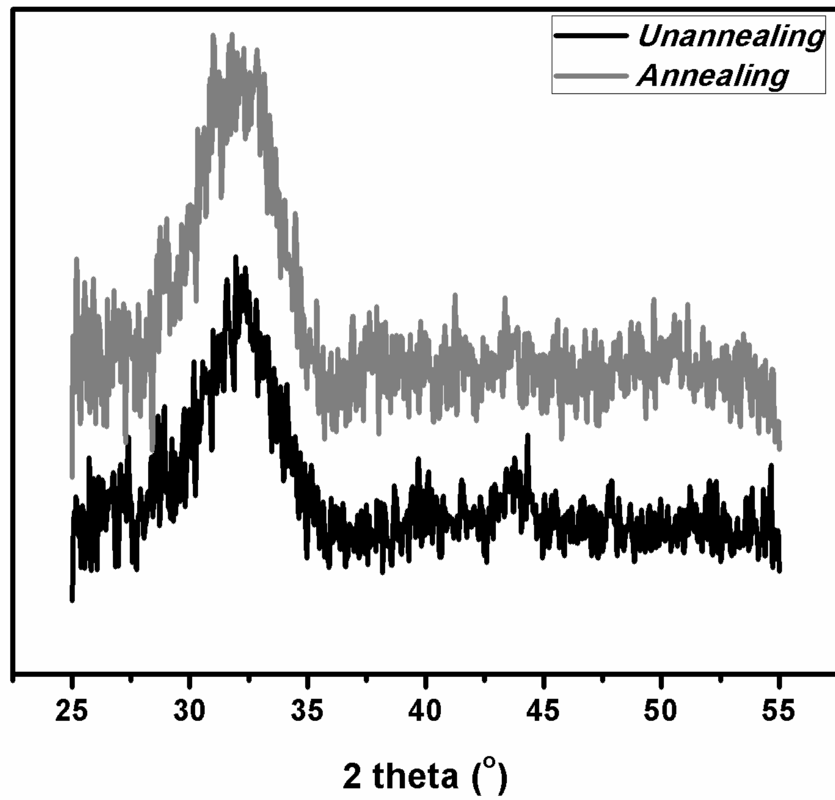

Figure 4. 9 XRD pattern of ITO film on PI substrate before and after stress measurement

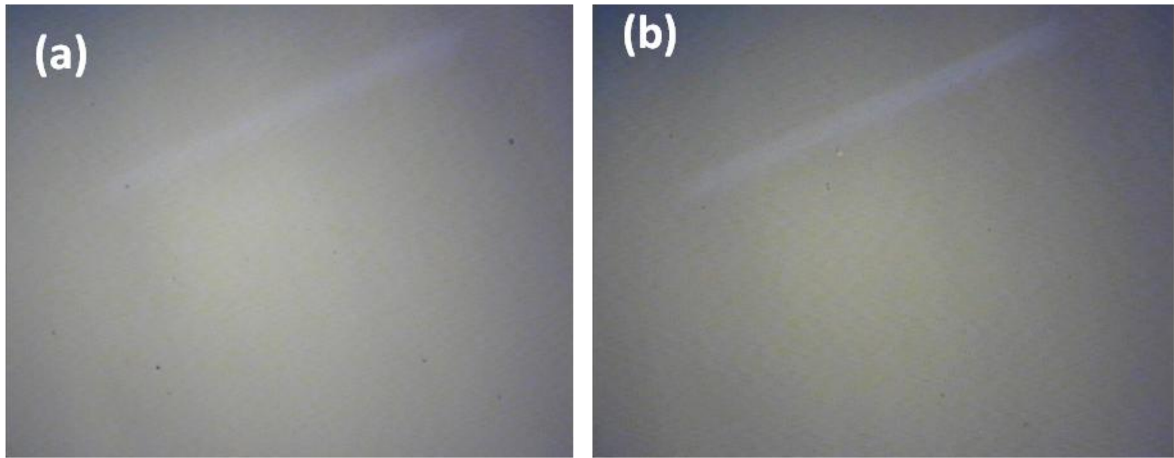

Figure 4. 10 Surface morphology of ITO/PI sample (a) before thermal cycling, and (b) after thermal cycling

4.3.4 Stress of ITO film deposited at 200 ℃ on PI substrate

The stress behavior of 200 ℃ deposited ITO/PI film stack is shown in Figure 4.11. Similar stress pattern of the ITO films deposited at room temperature and 200 ℃ indicates that the stress-temperature pattern of ITO film on PI substrate does not depend on the ITO deposition temperature. However, the stress values decreases with increasing substrate temperature. Table 4.3 summarizes the stresses of ITO film deposited at room temperature and 200 ℃. The initial stress of the ITO/PI sample in the latter case is 45 MPa, which is 10 MPa smaller than that in the former, 55 MPa. As mentioned in the previous section, the less tensile of ITO/PI stress with increasing ITO deposition temperature is due to an increase of bombarded energy.

At the end of the first heating process, the residual stress of ITO/PI deposited at 200 ℃ reaches 2 MPa, close to the zero point. The residual stress includes of thermal stress and intrinsic stress. Since the first component stress should be zero at film deposition temperature, the intrinsic stress of ITO/PI stack equals to its residual stress. The nearly zero point of the intrinsic stress indicates that ITO film and ODPA-BAPP polyimide substrate matches very well.

During the cooling period, the stress-temperature curve of 200℃-deposited ITO case is going linearly up with a slope of -0.335 MPa/℃. The ITO/PI residual stress reaches 60 MPa at the end of the first thermal cycling. A hysteresis stress of 15 MPa appears in the early

stress-temperature curve, which results from the rearrange of ITO atoms onto ODPA-BAPP polyimide substrate and the film grain growth.

In the second thermal cycling, as seen in Figure 4.11, the stress behavior of ITO/PI in both the second heating and cooling processes are the same as in the first cooling period. That reveals the ITO/PI stress is relieved completely because the system reaches a stable state after the first thermal cycle. The linearly stress-temperature curve in the second thermal cycle indicates the film stress is caused by the thermal origin.

It is observed from the OM images of ITO film before and after stress measurement (Figure 4.14) that there are no any damages on film surface during the measurement. It means the stress range of 2 – 60 MPa is still in the ITO film stress limitation.

As shown in Figure 4.7, the stress of ODPA-BAPP polyimide film on Si substrate is in the range of 5 – 52 MPa, while the stress values of ITO/PI in this case are in a larger range from 2 MPa to 60 MPa. It means the ITO film deposited at 200 ℃ on ODPA-BAPP polyimide may exhibit a compressive stress. As discussed in the case of Si substrate, the compressive stress in the ITO film is due to the better crystallinity of the film and the stronger particle bombardment. The XRD pattern in Figure 4.12 presents that the ITO film deposited on PI at room temperature is amorphous while the film deposited at 200 ℃ are crystalline with small peaks of (222), (400), and (440). It is clearly observed from the SEM images of ITO films deposited at room temperature and 200 ℃ on PI, in Figure 4.13, that the

200℃-deposited ITO film was formed from very large grains in the average size of 23 nm. The grains in 200 ℃-deposited ITO film site very closely may lead to an increase of the propulsive force among the grains, and then cause the film more compressive. This result matches with the case of ITO film deposited on Si substrate. It can be concluded that increasing the deposition temperature can reduce the ITO film tensile stress.

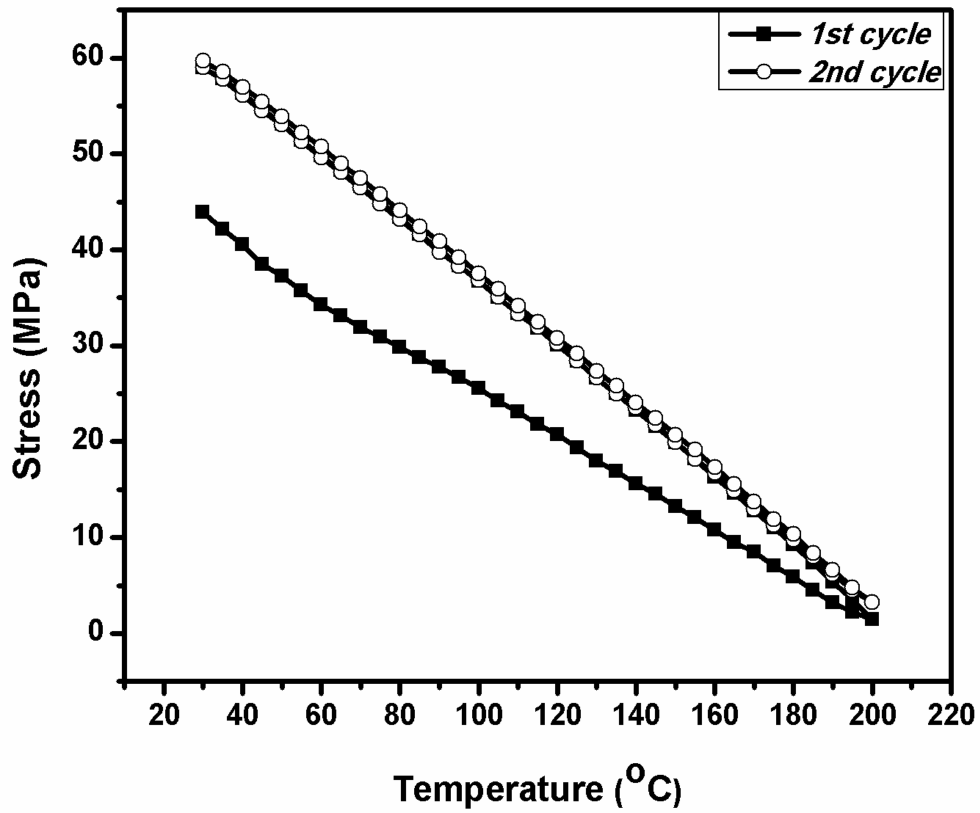

Figure 4. 11 Stress vs. temperature of ITO film deposited on ODPA-BAPP polyimide substrate at 200℃

Table 4. 3 Summary effect of substrate temperature on ITO/PI stress behavior

T_d	Stress range (MPa)	Initial stress (MPa)	Stress at RT (MPa)
RT	5 - 71	55	71
200℃	2 - 60	45	60

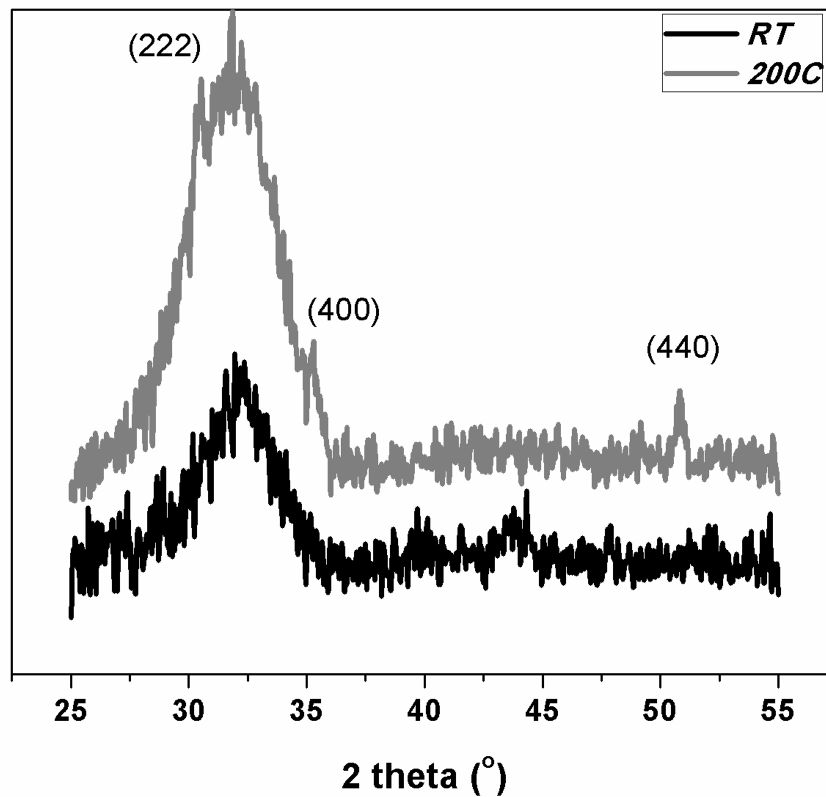

Figure 4. 12 XRD pattern of ITO deposited at room temperature and 200 ℃ on PI substrate

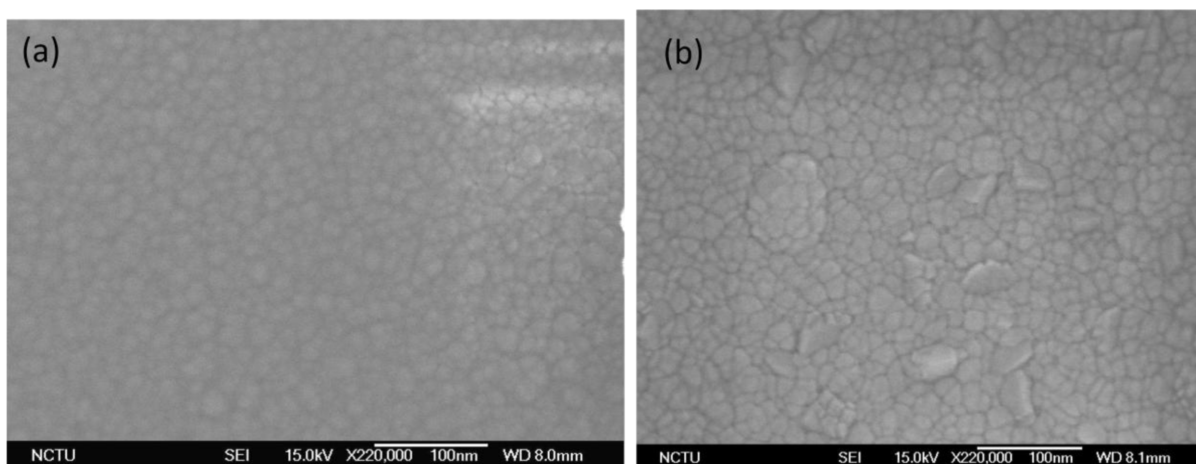

Figure 4. 13 SEM top-view of ITO film on ODPA-BAPP polyimide substrate: (a) Room temperature deposited film; (b) 200 ℃-deposited film

Figure 4. 14 Surface morphology of ITO/PI sample (a) as-deposited and (b) after the thermal cycling

4.4 Stress of ITO film on PET substrate

Stress of ITO film deposited on PET substrate is also studied in this thesis. However, the glass transition temperature of PET is quite low (70-80 ℃) such that ITO film was only deposited at room temperature. The stress measurement for both ITO/PET and PET on Si are carried out from 30 ℃ to 70 ℃ in order to maintain the quality of PET substrate and ITO/PET stack.

4.4.1 Stress of PET film on silicon substrate

To aid the stress analysis of ITO film, stress of a PET film on Si substrate was measured with two thermal cycles from room temperature to 70 ℃ in nitrogen ambient at 45 Torr.

The stress-temperature curve of the PET film on Si substrate is shown in Figure 4.15. Stress values of PET are in 0 - 10 MPa indicating that the film is under tensile stress. The evaporation of TFA solvent during the baking process and thermal curing is expected to cause the tensile stress in PET film.

In Figure 4.15, the initial stress value of the PET film is observed to be about 7 MPa. The residual stress drops down to 0 MPa with increasing temperature to 70℃ in the first heating process due to the thermal stress development. The coefficients of thermal expansion of PET film and silicon substrate are 50 ppm/℃ and 2.61 ppm/℃, respectively. Therefore,

PET film expands faster than the silicon substrate as temperature increases, resulting in a compressive film thermal stress ($\sigma_{th} < 0$) in the film as described in Eq. (4.2). The thermal stress development compensates for the intrinsic film stress, leading to a reduction in film residual stress.

When the heating temperature is over 60℃, the stress-temperature curve becomes flat and close to 0 MPa. This may due to the transformation from glassy state to rubbery state in the PET film. It is well recognized that above T_g, the coefficient of thermal expansion of PET significantly increases while its Young's modulus reduces to a small value, resulting in significant film stress change.

A tensile stress was built up monotonically during the cooling period from 70℃ to 30 ℃. This stress is due to the thermal expansion mismatch between the polymer film and silicon substrate and can be given by the Eq. (4.4):

$$\sigma_{th} = \frac{E_f}{1-\nu_f}(\alpha_s - \alpha_f)\Delta T \qquad (4.4)$$

Where, E_f, υ_f and α_f are the Young's modulus, Poisson ratio and coefficient of thermal expansion of the film, respectively. α_s is the coefficient of thermal expansion of the substrate. In this study, for PET film and Si substrate, E_f = 3.5 GPa, υ_f = 0.44, α_f = 50 ppm/ ℃, and α_s = 2.61 ppm/ ℃. The thermal stress of film at 70 ℃ is calculated to be equal - 11.85 MPa. The "-" indicates the thermal stress is compressive. The linear behavior of the PET film stress shown

in Figure 4.15 implies that the term of $\{[E_f/(1-\nu_f)](\alpha_s-\alpha_f)\}$ is approximately a constant (~ -0.240 MPa/℃) between 30℃ and 70℃. This experimental result matches with the calculation result.

The stress behavior upon the repeated thermal cycling is reproducible and approximately linear in temperature, suggesting the stress observed is thermal in origin[72].

The stress-temperature curve of PET film reaches stable state after two thermal cycles and obtains a stress value of 10 MPa at room temperature. The stress was relieved -3 MPa caused by the TFA solvent evaporation and the possibly phase transformation in PET film.

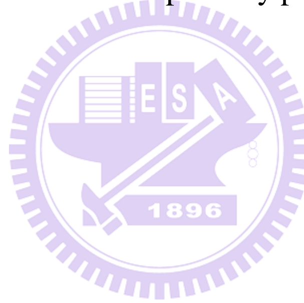

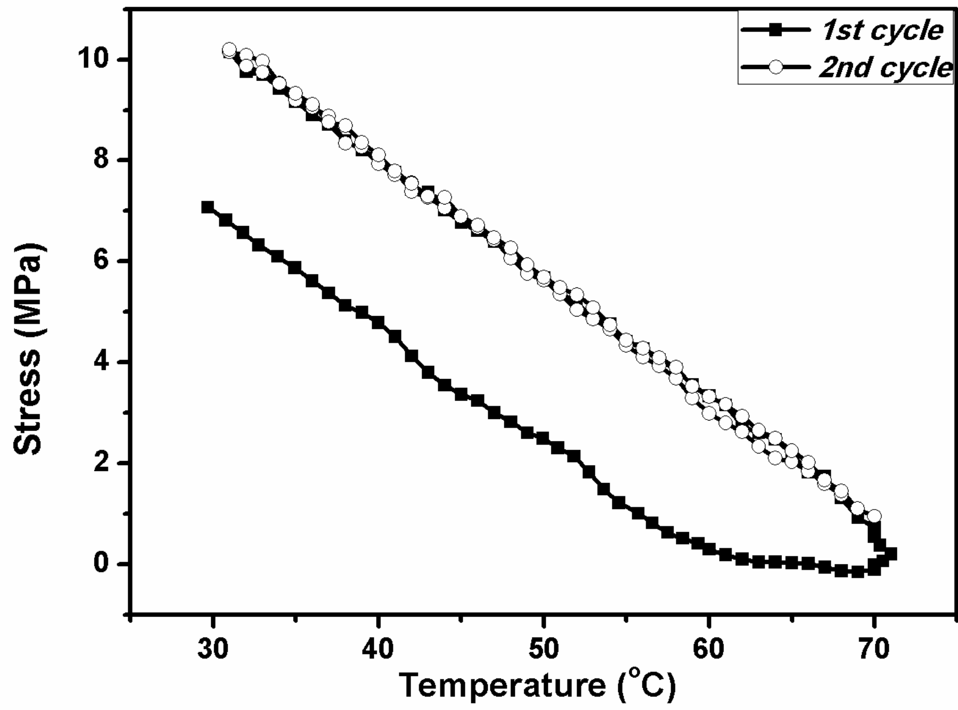

1896

Figure 4. 15 Stress vs. temperature of PET film on Si substrate

4.4.2 Stress of ITO film deposited at room temperature on PET substrate

Figure 4.16 shows the stress-temperature curve of ITO/PET sample, which starts from 30℃, 13 MPa onwards, showing the presence of a tensile initial stress (i.e. a concave wafer). It is also observed that the stress decreases with increasing temperature. It is due to the thermal stress development at the film – substrate interface. Both PET and ITO expand more than silicon wafer thus the wafer tends to less concave with increasing temperature. However, as temperature increases above 60℃, the PET film tends to change in phase morphology followed by an extreme expansion compared to the ITO film; and the substrate also becomes much softer. The difference in the thermal expansion between ITO and PET induces a force makes PET bend toward to ITO side. On the other hand, the PET substrate expands much more than the Si wafer. This also generates a force which pulls the PET film bend to Si side. The trade-off between those two forces causes the ITO/PET multilayer bending and results in a change of the film stress. The increase in tensile stress of ITO film, i.e the ITO/PET multilayer is bent toward to the ITO side, indicates the force by the ITO-side is greater than the Si-side. The ITO/PET stress achieves a value of 8 MPa at 70℃. After that, the sample was cooled down to room temperature. A linear tensile stress was built up with the slope of -0.266 MPa/℃ during the cooling cycle. The film stress at room temperature after the first thermal cycle is 18.5 MPa. And, the relief stress is - 5.5 MPa after two thermal cycles.

In Figure 4.15, the stress-temperature plot of PET film on silicon substrate shows a

stress hysteresis during the first thermal cycling. In addition, the treatment temperature is in range of 30 – 70℃, which is quite low to reveal any structure change in ITO film, but is high enough to alter the morphology of PET substrate. Thus, the stress hysteresis phenomenon appears in the first stress-temperature curve of ITO/PET can be attributed to the phase transformation in the PET substrate. However, the stress hysteresis in the case of the PET with ITO film is 3 MPa larger than in the case of the PET without ITO. PET is a compliant substrate with low Young's modulus ~ 3.5 GPa. Thus, the larger stress hysteresis in ITO/PET compared to PET, may be induced by the plastic deformation of PET substrate under the stress between ITO and PET. This results in a large stress relief of ITO/PET sample during the thermal cycling.

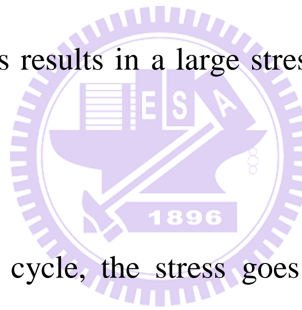

During the second thermal cycle, the stress goes down and up monotonically with temperature increase and decrease, respectively. There is a little stress hysteresis occurs in this cycle. This indicates that the film state reaches a stable state. The film stress in the second thermal cycle is caused by the thermal origin only.

The surface morphology of ITO on PET substrate was inspected by the optical microscope. Figure 4.17 shows that no any cracking or delamination occurred during the stress measurement within 30 – 70 ℃.

Compared to the stress-temperature curve of the PET film on silicon substrate, the

stress values of PET with ITO are 5 – 9 MPa higher. The ITO film deposited onto PET substrate is under a tensile stress, indicating that the ITO film is stretched when deposited on PET substrate.

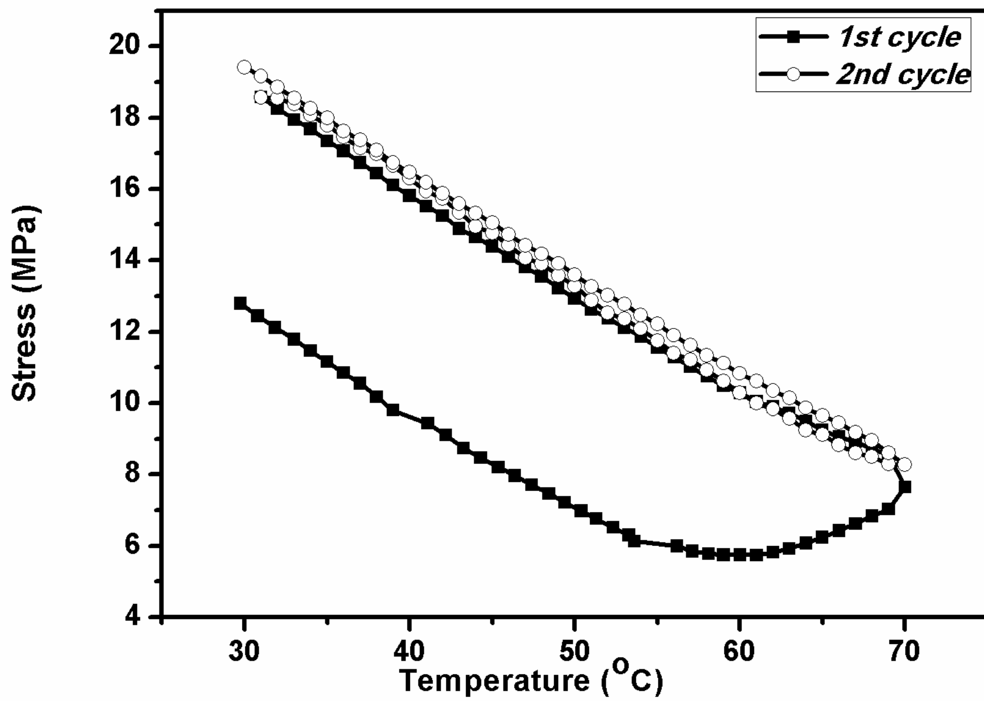

Figure 4. 16 Stress-temperature curve of ITO film deposited at room temperature onto PET substrate.

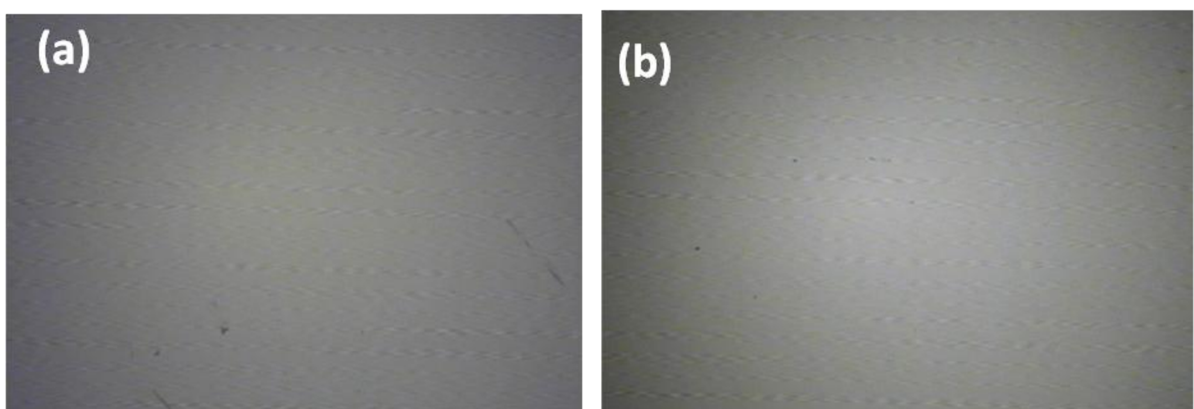

Figure 4. 17 Surface morphology of ITO/PET sample (a) as-deposited and (b) after thermal cycling

4.5 Effect of substrates on the stress of ITO film

In substrate point of view, stress values of room temperature deposited ITO films on various substrates, such as Si, PI, and PET are listed in Table 4.4. Stress values of ITO on Si range from 80 MPa to 330 MPa. Stress values of ITO/PI on Si range from 5 to 71 MPa. Finally, ITO/PET on Si is under the least stress values from 6 to 18.5 MPa. The stress levels of ITO/PET on Si and ITO/PI on Si are both lower than that of ITO on Si, specifically, 93 % and 76 % lower, respectively. As mentioned in Section 4.3, it is believed that the stress reduction in ITO films deposited on polymer substrates is due to the ITO/polymer interface deformation [72]. Si is a rigid substrate with high Young's modulus, 131 GPa, thus it very hard for Si to deform under the ITO film stress. However, both PET and PI are compliant substrates with very low Young's moduli, 3.5 GPa and 5.6 GPa, respectively. These polymer substrates can be easily deformed under the ITO film stress, resulting in the film stress reduction. Between PET and PI substrates, PET is softer than PI. Thus, PET can be deformed more than PI such that the stress of ITO film on PET is reduced more than ITO on PI. Therefore, ITO/PET sample is under lower stress level than ITO/PI sample. Through Figures 4.1, 4.8 and 4.16, it is observed that stress vs. temperature curves of ITO/PET and ITO/PI stacks show an elastic behavior after one thermal cycle while stress vs. temperature curve of ITO on Si has not shown the elastic behavior even after two thermal cycles. That indicates the polymer presence aid the stack easily obtain a stable state. It is due to the fact that the PET

and PI are bendable. Thus, these polymer substrates easily deform to match with the ITO films. In contrast, Si is a rigid and unbendable substrate, thus ITO on Si needs some thermal cycles to obtain a stable state.

Table 4. 4 Summary stress of ITO films on various substrates

Samples	Stress range (MPa)	Initial stress (MPa)	Stress at RT after thermal cycling (MPa)
ITO/Si	80 – 330	185	330
ITO/PI/Si	5 – 71	55	71
ITO/PET/Si	6 – 18.5	13	18.5

ES A 1896

4.6 Critical stress for damage of ITO film on polymer substrates

Stress measurement of ITO films on polymer substrates was carried out from 30 ℃ to the temperature above the polymers' T_g (100 ℃ for ITO/PET and 250 ℃ for ITO/PI) to test if cracking or delamination occurs in ITO film and to obtain the critical stress for film damages.

Figure 4.18 shows stress vs. temperature curve within 30 – 100 ℃ of ITO film on PET substrate. The stress behavior of ITO film at temperatures below 70 ℃ in the heating process is similar to what was discussed in Section 4.4. However, when the temperature exceeds the T_g of PET (~ 75 ℃), the film stress was relaxed much more due to the significant expansion of PET. Then, the film stress goes up as sample was cooled. The stress vs. temperature curve drastically changes its slope at 35 ℃ and stress value of 19.2 MPa. It means the film was damaged at that point because the film was under large stress. The optical microscope image shown in Figure 4.19 points out that the film was cracked after thermal cycling. It can be defined that the critical stress for cracking of ITO/PET is 19.2 MPa.

ITO/PI stress behavior from room temperature to 250 ℃ is shown in Figure 4.20. It is observed that the slope of stress vs. temperature curve decreases drastically when temperature is cooled down to 50 ℃. The OM images of ITO film surface were taken before and after the stress measurement and are shown in Figure 4.21. There are some cracking of film surface after the thermal cycling measurement (Figure 4.21b). The cracking is believed to cause the slope of stress vs. temperature curve change at 50 ℃ in the cooling cycle. The stress value at

that point is 75 MPa, which is defined as critical stress for cracking of ITO/PI.

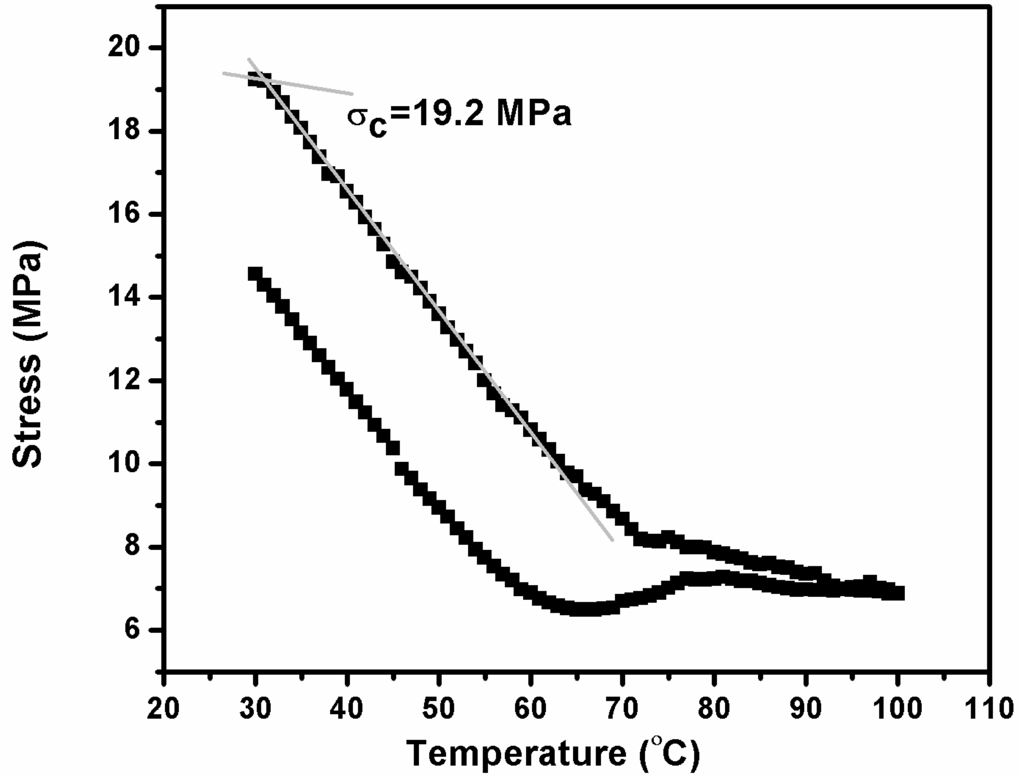

Figure 4. 18 Stress vs. temperature of ITO on PET within 30 – 100 ℃

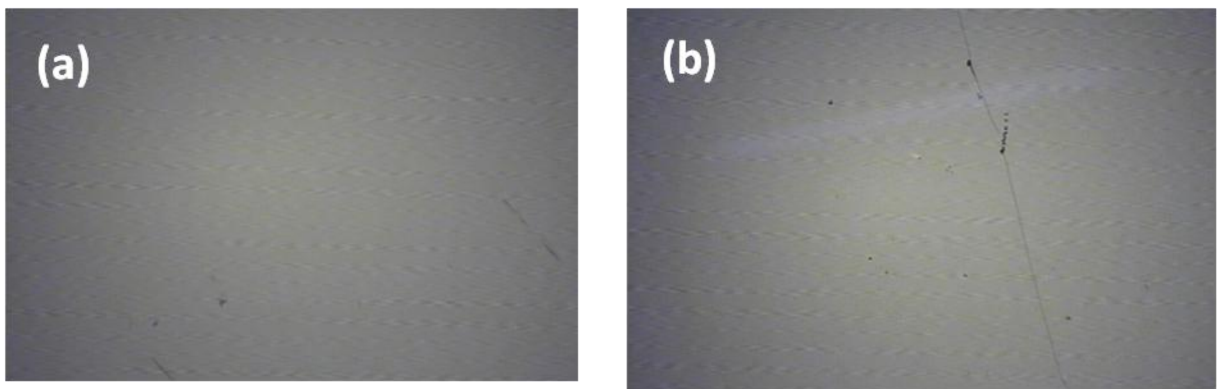

Figure 4. 19 Surface morphology of ITO/PET (a) before stress measurement and (b) after stress measurement within 30 – 100 ℃

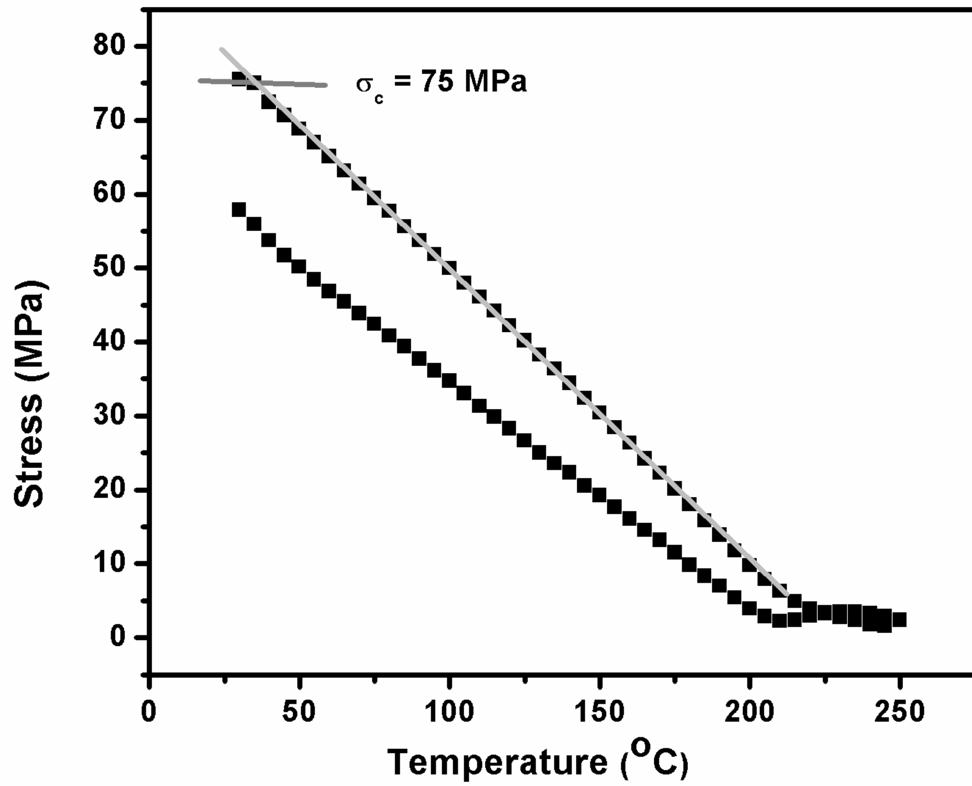

Figure 4. 20 Stress vs. temperature of ITO/PI within 30 – 250 ℃

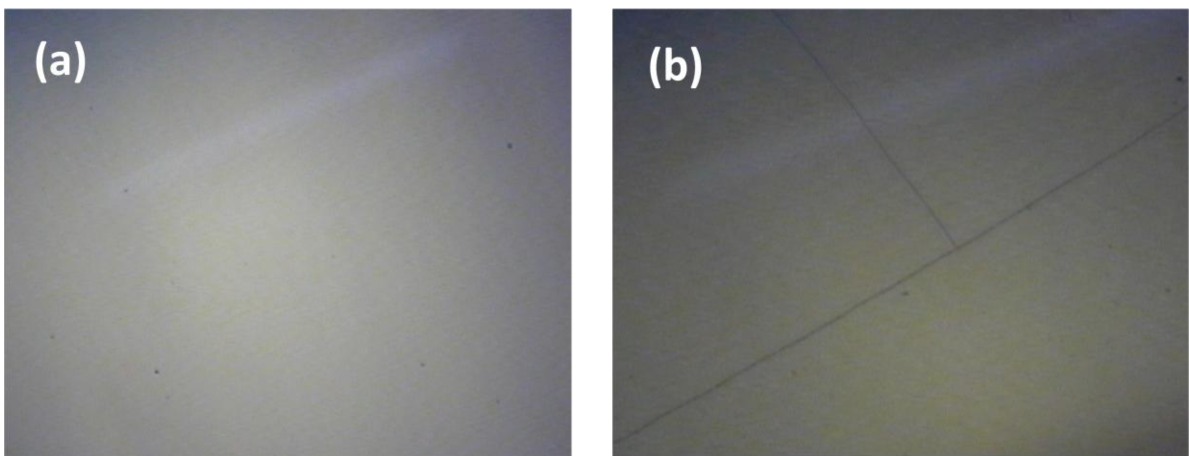

Figure 4. 21 Surface morphology of ITO/PI (a) before stress measurement and (b) after stress measurement within 30 – 250 ℃

4.7 Effects of substrate on the optical properties of ITO films

The transmittance of ITO films deposited at room temperature on glass, PET and ODPA-BAPP PI substrates were measured by employing the UV-visible spectrophotometer system. Figure 4.22 shows that the transmittances of ITO films on these substrates are not much different. Namely, the transmittance of ITO on glass is 89 %, ITO on PET is 88 %, and ITO on PI is 86 %.

The band gap energy, E_g, is determined by using the absorption coefficient following the correlation given by Eq. (4.5)[73]

$$\alpha \propto (h\nu - E_g)^{1/2} \qquad (4.5)$$

Where α is the absorption coefficient, $h\nu$ is the photon energy, E_g is the optical band gap. The optical band gap can be estimated by plotting α^2 vs. $h\nu$, then extrapolating the straight line portion of the energy axis[74] as posed in Figure 4.23, which shows the band gap of ITO on glass, PET and PI substrates. As mentioned in Chapter 2, the optical band gap is described by Eq. 4.6

$$E_g = E_{gi} + \frac{\pi^2 \hbar^2}{2m^*_{VC}} \left(\frac{3N}{\pi}\right)^{2/3} \qquad (4.6)$$

Where E_{gi} is the intrinsic energy band gap.

Figure 4.25 illustrates the optical band gaps of ITO/glass, ITO/PET, and ITO/PI, which are 3.43, 3.33, and 3.29 eV, respectively. It is clear that ITO on polymer substrates has a narrower band gap. The band gap of ITO on PET is lager than that of ITO on PI. As given

in Eq. (4.6), the film band gap is controlled by the carrier concentration and the reduced effective mass. The carrier concentrations of ITO on these substrates, listed in Table 4.5, are similar. Thus, the effect of this factor on ITO band gap can be ignored. The smaller optical band gap of ITO/PI is believed to cause from the higher tensile stress of ITO/PI compared to ITO/PET (See Table 4.5), which induces the effective masses of carriers in the conduction and valence bands, m^*_C and m^*_V, respectively [75]. These effective masses and the reduced effective mass, m^*_{VC}, are interdependent as described in Eq. 4.7. Therefore, when m^*_C and m^*_V increase, m^*_{VC} is also increase, resulting in narrowing of the band gap by Equation (4.6).

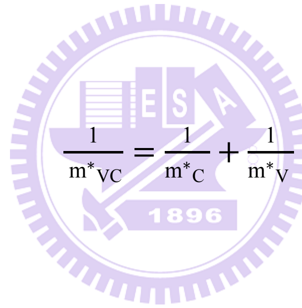

$$\frac{1}{m^*_{VC}} = \frac{1}{m^*_C} + \frac{1}{m^*_V} \qquad (4.7)$$

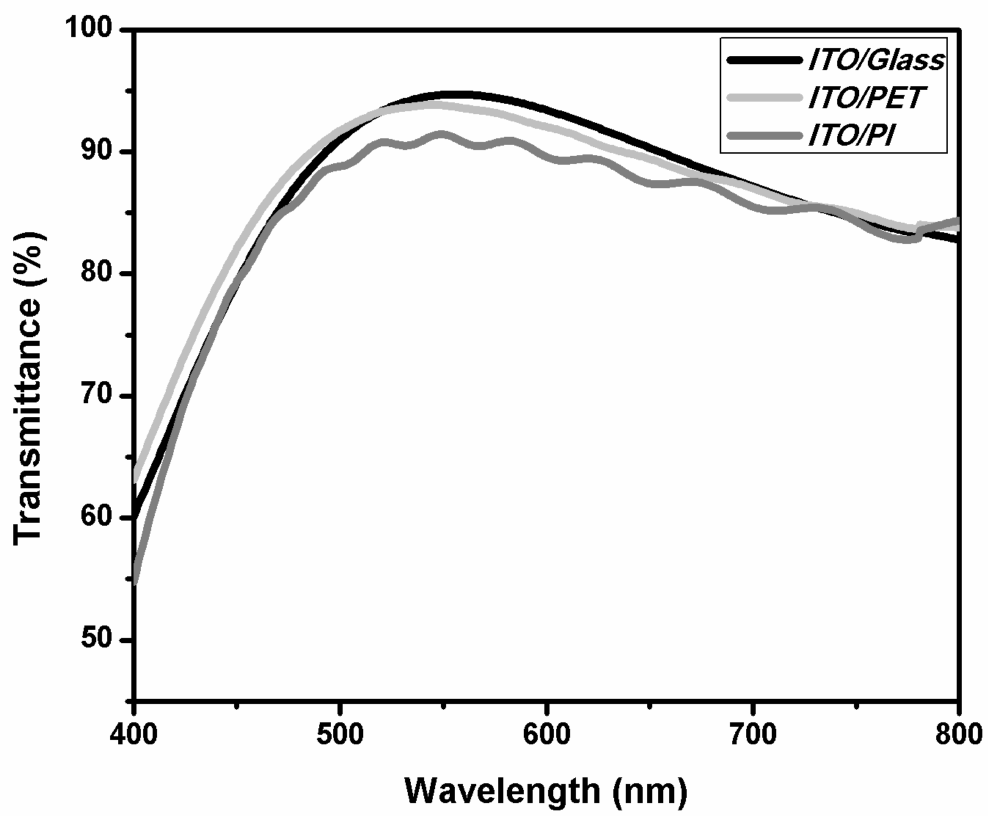

1896

Figure 4. 22 Transmittance of ITO films on glass, PET and PI in the visible light

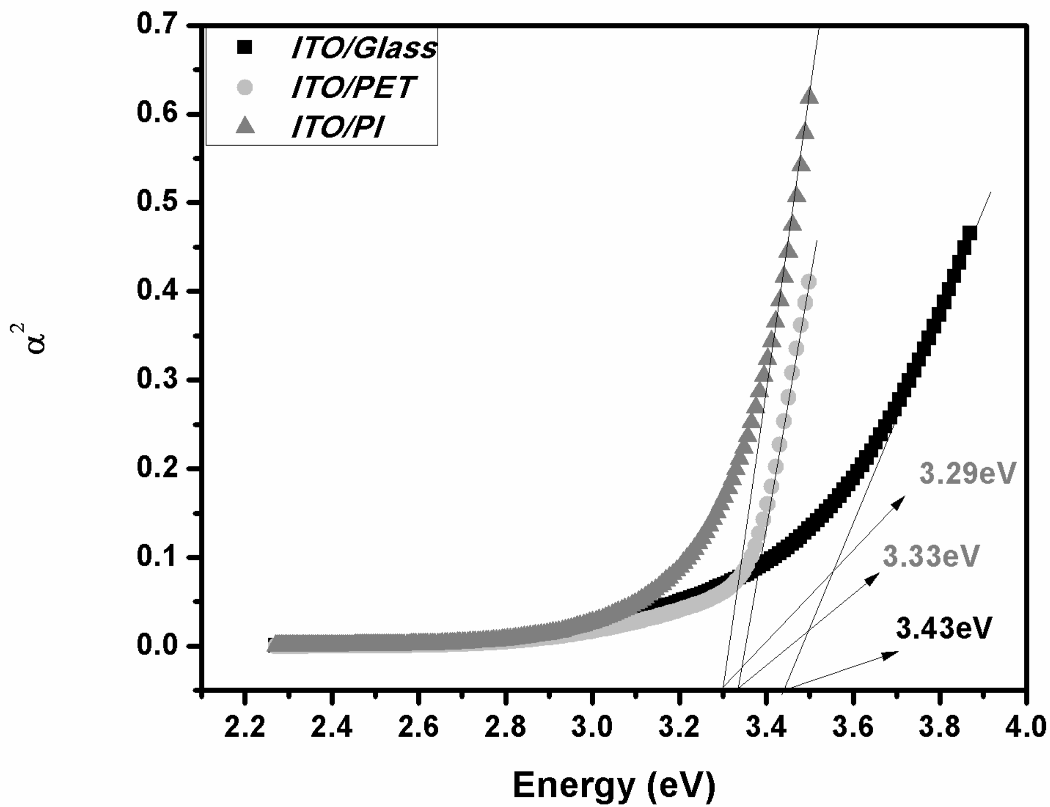

Figure 4. 23 Optical band gap of ITO film on glass, PET and PI substrates

Table 4. 5 Optical band gap of ITO in the relationship with film stress and carrier concentration

	Band gap (eV)	Stress (MPa)	Carrier concentration (10^{20} cm^{-3})
ITO/PET	3.33	13	1.14
ITO/PI	3.29	55	1.68

Chapter 5 Conclusion

Stress built-up in the ITO film, which serves as a transparent conducting layer in many optoelectric devices, is an inevitable occurrence, depending on its deposition method and the themomechanical mismatch between ITO film and substrate materials. The stress may result in film cracking or buckling, leading to poor device durability and reducing its optical and electrical properties. The stress behavior in the layered structure will be quite different when polymer materials with large CTE and weaker modulus are used as the substrate in replacement of conventional glass or silicon substrate. This issue is of significant interest as the demand for flexible optoelectric devices intensifies recently. Therefore, it is important to understand the stress behavior of ITO film deposited at different temperatures on the Si and polymer substrates and under multiple thermal cycling. In addition, their impact on the thermomechanical integrity of the ITO/substrate layered structure will be assessed and discussed. The critical stress value for damages of ITO films deposited on polymer substrates, such as PET and ODPA-BAPP polyimide, was also investigated. Finally, the effect of substrate on optical properties of ITO film was studied.

The ITO film stress as a function of temperature was obtained by using a bending beam technique. The results show that ITO films deposited at room temperature on Si, PET and PI substrates are under tensile stress. The stress level of ITO film/substrate depends on the

Young's modulus of substrate. The film, which was deposited on a soft substrate such as PET and PI, bears a low level stress because the soft substrate can plastically deform, resulting in a stress reduction. The softer substrate, the more stress reduction of the film. Therefore, the ITO films on PET and PI substrates are under lower stress than ITO film on Si substrate. Stress of ITO/PET is in the lowest level due to PET's lowest Young's modulus. In contrast, Si has highest Young's modulus, resulting in the highest stress level of ITO on Si. When the film stress measurement was carried out over the glass transition temperatures of the polymer substrates, the cracking phenomenon occurred for both ITO/PET and ITO/PI samples. The critical stress values for film cracking are 19.2 MPa for ITO/PET and 75 MPa for ITO/PI. That means ITO/PI can bear a higher stress level than ITO/PET.

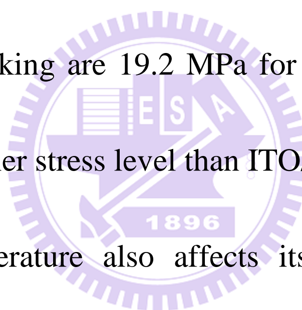
ESA 1896

ITO film deposition temperature also affects its microstructure and stress. With increasing ITO deposition temperature, the atomic peening effect during the film growth process becomes stronger and the crystallinity of ITO film is improved. Thus, the stress tendency of ITO film on both Si and ODPA-BAPP polyimide is more compressive compared to the ITO film deposited at room temperature.

Optical properties of ITO/PET and ITO/PI were also studied by UV-visible spectrophotometer system to understand any substrate effect. The transmittance of ITO on glass, PET and PI are similar. However, ITO films on polymer substrate show a narrowing in the optical band gap. Specifically, the optical band gap of ITO/PI is smaller than that of

ITO/PET. It is presumably due to the more tensile of ITO stress when the film deposited on PI.

References

[1] C. Guille'n and J. Herrero, Thin Solid Films **431-432**, 403 (2003).

[2] K. Tvingstedt and O. Inganäs, Adv. Mater. **19**, 2893 (2007).

[3] Q. Liu, J. Mao, Z. Liu, N. Zhang, Y. Wang, L. Yang, S. Yin, and Y. S. Chen, Nanotechnology **19**, 115601 (2008).

[4] H. L. Wang, W. Y. Ding, C. Q. Liu, and W. P. Chai, Chin. Phys. Lett. **27**, 127302 (2010).

[5] M. Wakagia, K. Chaharaa, K. Onisawaa, Y. Kawakubob, T. Kichikawab, T. Satohb, and T. Minemuraa, Thin Solid Films **411**, 46 (2002).

[6] H. Kajii, T. Taneda, and Y. Ohmori, Thin Solid Films **438-439**, 334 (2003).

[7] X. Y. Deng, Int. J. Mol. Sci. **12**, 1575 (2011).

[8] Y. Z. You, Y. S. Kim, D. H. Choi, H. S. Jang, J. H. Lee, and D. Kim, Materials Chemistry and Physics **107**, 444 (2008).

[9] H. J. Park, J. W. Park, S. Y. Jeong, and C. S. Ha, Proceedings of the IEEE **93**, 1447 (2005).

[10] S. H. K. Park, J. I. Lee, C. S. Hwang, and H. Y. Y. Chu, Jpn. J. Appl. Phys. **44**, L242 (2005).

[11] G. Sonia, L. Jay, V. Eric, and T. Dorota, Thin Solid Films **515**, 4745 (2007).

[12] H. Han, D. Adams, J. W. Mayer, and T. L. Alford, J. Appl. Phys. **98**, 083705 (2005).

[13] K. Hermona, C. Pandya, V. Subramania, and K. Changhee, Synth. Met. **157**, 120 (2007).

[14] G. F. Wang, X. M. Tao, and H. M. Huang, Appl. Surf. Sci. **253**, 4463 (2007).

[15] Y. Zhang, J. M. Zhang, Y. L. Lu, Y. X. Duan, S. K. Yan, and D. Y. Shen, Macromolecules **37** (7), 2532 (2004).

[16] P. J. Cygan, J. P. Zheng, S. P. S. Yen, and T. R. Jow, Electrical Insulation and Dielectric Phenomena, 1993. Annual Report., 630, Pocono Manor, PA, USA, 17 - 20th Oct. 1993.

[17] C. T. Chen, T. S. Hsu, R. J. Jeng, and H. C. Yeh, Journal of Polymer Science: Part A: Polymer Chemistry **38**, 498 (2000).

[18] R. Glang, R. A. Holmwood, and R. L. Rosenfeld, The Review of Scientific Instruments **36** (1), 7 (1965).

[19] S. K. Hong, H. J. Kim, and H. G. Yang, J. Appl. Phys. **80**, 822 (1996).

[20] A. Rajamani, R. Beresford, and B. W. Sheldon, Appl. Phys. Lett. **79**, 3776 (2001).

[21] B. W. Sheldon, K. H. A. Lau, and A. Rajamani, J. Appl. Phys. **90**, 5097 (2001).

[22] Y. Q. Fua, H. Dua, and S. Zhang, Surface and Coating Technology **167**, 120 (2003).

[23] E. Mounier and Y. Pauleau, Diamond and Related Materials **6**, 1182 (1997).

[24] S. Chowdhury and M. T. Laugier, Appl. Surf. Sci. **253**, 4289 (2007).

[25] J. H. Zhao, T. Ryan, P. S. Ho, A. J. Mckerrow, and W. Y. Shih, J. Appl. Phys. **88**, 5 (2000).

[26] H. Nomura and M. Asano, Jpn. J. Appl. Phys. **34**, 6143 (1995).

[27] S. K. Choi and J. I. Lee, J. Vac. Sci. Technol. A **19**, 2043 (2001).

[28] M. Ohring, Material Science of Thin Films: deposition and structure, second edition, Sandiego, USA (2002).

[29] P. F. Carcia, R. S. McLean, M. H. Reilly, Z. G. Li, L. J. Pillione, and R. F. Messier, Appl. Phys. Lett. **81**, 1800 (2002).

[30] E. Nishimura, T. Sasabayashi, N. Ito, Y. Sato, K. Utsumi, K. Yano, A. Kaijo, K. Inoue, and Y. Shigesato, Jpn. J. Appl. Phys. **46**, 7806 (2007).

[31] K. S. Chen, X. Zhang, and S. Y. Lin, Thin Solid Films **434**, 190 (2003).

[32] P. F. Carcia, R. S. McLean, M. H. Reilly, Z. G. Li, L. J. Pillione, and R. F. Messier, J. Vac. Sci. Technol. A **21**, 745 (2003).

[33] H. Windischmann, J. Appl. Phys. **62**, 1800 (1987).

[34] Klockholm and Berry, J. Electrochem. Soc. **115**, 823 (1968).

[35] S.T.Chen, C.H.Yang, F.Faupel, and P.S.Ho, J. Appl. Phys. **64**, 6690 (1988).

[36] H. Tetsuka, T. Ebina, T. Tsunoda, H. Nanjo, and F. Mizukami, Surface and Coating Technology **202**, 2955 (2008).

[37] V. Craciun, D. Craciun, X.Wang, T. J. Anderson, and R. K. Singh, Journal of

Optoelectronics and Advanced Materials **5**, 401 (2003).

[38] L. Meng and M. P. Dossantos, Vacuum **45**, 1191 (1994).

[39] H. Kim, C. M. Gilmore, A. Pique, J. S. Horwitz, H. Mattoussi, H. Murata, Z. H. Kafafi, and D. B. Chrisey, J. Appl. Phys. **86**, 6451 (1999).

[40] K. Zhang, F. Zhu, C. H. Huan, and A. T. Wee, J. Appl. Phys. **86**, 974 (1999).

[41] H. N. Cui, V. Teixeira, and A. Monteiro, Vacuum **67**, 589 (2002).

[42] J. C. C. Fan and J. B. Goodenough, J. Appl. Phys. **48**, 3524 (1977).

[43] N. Balasubramanian and A. Subrahmanyam, J. Appl. Phys. **22**, 206 (1989).

[44] W. G. Haines and S. A. Knickerbcker, J. Appl. Phys. **54**, 3497 (1983).

[45] F. O. Adurodijia, H. Izumi, T. Ishihara, H. Yoshioka, and M. Motoyama, J. Appl. Phys. **88**, 4175 (2000).

[46] Y. Q. Fu, H. J. Du, and S. Zhang, Surface and Coating Technology **167**, 120 (2003).

[47] J. S. Lee and J. W. Park, Journal of Materials Science Letter **16**, 941 (1997).

[48] Y. C. Lin, W. Q. Shi, and Z. Z. Chen, Thin Solid Films **517**, 1701 (2009).

[49] A. Užupis, S. Tamulevičius, R. Butkutė, Vengalis, and V. Lisauskas, Phys. Stat. Sol. C **1**, 307 (2004).

[50] B. Vengalis, A. Maneikis, F. Anisimovas, R. Butkute, L. Dapkus, and A. Kindurys, Journal of Magnetism and Magnetic Materials **211**, 35 (2000).

[51] J. Lappalainen, J. Frantti, J. Hiltunen, V. Lantto, and M. Kakihana, Ferroelectrics **335**,

149 (2006).

[52] H. S. Moon, W. Lee, P. J. Reucroft, and J. W. Park, Journal of Power Sources **119-121**, 710 (2003).

[53] C. Sujatha, G. M. Rao, and S. Uthanna, Materials Science and Engineering B **94**, 106 (2002).

[54] D. R. Cairns, S. M. Sachsman, D. K. Sparacin, R. P. Witte, G. P. Crawford, and D. C. Paine, Mat. Res. Soc. Symp. Proc. **594**, 401 (2000).

[55] G. S. Heo, I. G. Gim, H. K. Lee, J. H. Song, and T. W. Kim, Jnp. J. Appl. Phys. **49**, 031104 (2010).

[56] T. N. Ng, W. S. Wong, R. A. lujan, and R. A. Street, Adv. Mater. **21**, 1855 (2009).

[57] M. Chu, Y. Sun, U. Aghoram, and S. E. Thompson, Annu. Rev. Mater. Res. **39**, 203 (2009).

[58] S. N. Huang, National Chiao-Tung University, Master's degree, Taiwan, 2009.

[59] J. H. Zhao, T. Ryan, and P. S. Ho, J. Appl. Phys. **85** (9), 6421 (1999).

[60] Y. Du, J. H. Zhao, and P. Ho, Journal of Electronic Packaging **123**, 196 (2001).

[61] D. McMullan, Work report, University of Cambridge, UK, 1993.

[62] J. A. Smith, Phys. Educ. **17**, 111 (1982).

[63] T. Y. Lin., unpulished data, National Chiao-Tung University, Taiwan.

[64] S. X. Hu, unpulished data, National Chiao-Tung University, Taiwan.

[65] Dupont Kapton Polyimide Film General Specifications, Bulletin GS-97-7.

[66] V. Bhatt, S. Chandra, S. Kumar, C. M. S. Rauthan, and P. N. Dixit, Indian Journal of Pure and Applied Physics **45**, 377 (2007).

[67] J. Chen and J. A. Barnard, Materials Science and Engineering A **191**, 233 (1995).

[68] J. H. Lee, J. Electroceram **23**, 554 (2009).

[69] E. Terzini, G. Nobile, S. Loreti, C. Minarini, T. Polichetti, and P. Thilakan, Jpn. J. Appl. Phys. **38**, 3448 (1999).

[70] H. Morikawa and M. Fujita, Thin Solid Films **359**, 61 (2000).

[71] W. Chung, M. O. Thompson, P. Wickboldt, D. Toet, and P. G. Carey, Thin Solid Films **460**, 291 (2004).

[72] S. T. Chen, C. H. Yang, F. Faupel, and P. S. Ho, J. Appl. Phys. **64**, 6690 (1988).

[73] H. Han, J. W. Mayer, and T. L. Alford, J. Appl. Phys. **100**, 083715 (2006).

[74] H. Kim, J. S. Horwitz, G. P. Kushto, and Z. H. Kafari, Appl. Phys. Lett. **79**, 284 (2001).

[75] G. Liu, Y. Chen, C. Jia, G. D. Hao, and Z. G. Wang, J. Phys.: Condens. Matter **23**, 015801 (2011).